The Gakkel Ridge: Bathymetry, gravity anomalies, and crustal accretion at extremely slow spreading rates

James R. Cochran,[1] Gregory J. Kurras,[2] Margo H. Edwards,[3] and Bernard J. Coakley[4,5]

Received 12 February 2002; revised 20 July 2002; accepted 4 October 2002; published 22 February 2003.

[1] The Gakkel Ridge in the Arctic Ocean is the slowest spreading portion of the global mid-ocean ridge system. Total spreading rates range from 12.7 mm/yr near Greenland to 6.0 mm/yr where the ridge disappears beneath the Laptev Shelf. Swath bathymetry and gravity data for an 850 km long section of the Gakkel Ridge from 5°E to 97°E were obtained from the U.S. Navy submarine USS *Hawkbill*. The ridge axis is very deep, generally 4700–5300 m, within a well-developed rift valley. The topography is primarily tectonic in origin, characterized by linear rift-parallel ridges and fault-bounded troughs with up to 2 km of relief. Evidence of extrusive volcanic activity is limited and confined to specific locations. East of 32°E, isolated discrete volcanoes are observed at 25–95 km intervals along the axis. Abundant small-scale volcanism characteristic of the Mid-Atlantic Ridge (MAR) is absent. It appears that the amount of melt generated is insufficient to maintain a continuous magmatic spreading axis. Instead, melt is erupted on the seafloor at a set of distinct locations where multiple eruptions have built up central volcanoes and covered adjacent areas with low relief lava flows. Between 5°E and 32°E, almost no volcanic activity is observed except near 19°E. The ridge axis shoals rapidly by 1500 m over a 30 km wide area at 19°E, which coincides with a highstanding axis-perpendicular bathymetric high. Bathymetry and side scan data show the presence of numerous small volcanic features and flow fronts in the axial valley on the upper portions of the 19°E along-axis high. Gravity data imply up to 3 km of crustal thickening under the 19°E axis-perpendicular ridge. The 19°E magmatic center may result from interaction of the ridge with a passively imbedded mantle inhomogeneity. Away from 19°E, the crust appears thin and patchy and may consist of basalt directly over peridotite. The ridge axis is continuous with no transform offsets. However, sections of the ridge have distinctly different linear trends. Changes in ridge trend at 32°E and 63°E are associated with a set of bathymetric features that are very similar to each other and to inside/outside corner complexes observed at the MAR including highstanding "inside corner" ridges, which gravity data show to be of tectonic rather than magmatic origin. *INDEX TERMS:* 3035 Marine Geology and Geophysics: Midocean ridge processes; 3010 Marine Geology and Geophysics: Gravity; 9315 Information Related to Geographic Region: Arctic region; *KEYWORDS:* Gakkel Ridge, mid-ocean ridge, oceanic crust, volcanic emplacement, Arctic Ocean, Eurasian Basin

Citation: Cochran, J. R., G. J. Kurras, M. H. Edwards, and B. J. Coakley, The Gakkel Ridge: Bathymetry, gravity anomalies, and crustal accretion at extremely slow spreading rates, *J. Geophys. Res.*, *108*(B2), 2116, doi:10.1029/2002JB001830, 2003.

1. Introduction

[2] The ultraslow spreading Gakkel Ridge forms the North America–Eurasia plate boundary in the Arctic. It extends for 1800 km across the Eurasian basin of the Arctic Ocean from the Spitzbergen transform system near the northeastern tip of Greenland to the continental margin of Siberia near 125°E (Figure 1), and continues into the continent as a broad region of continental rifting on the Laptev shelf. The Gakkel Ridge is the slowest spreading portion of the global mid-ocean ridge system (Figure 2). Extensive aeromagnetic studies of the Eurasian Basin have found a pattern of lineated ridge-parallel magnetic anomalies

[1]Lamont-Doherty Earth Observatory of Columbia University, Palisades, New York, USA.
[2]Department of Geology and Geophysics, School of Ocean Earth Science and Technology, University of Hawaii, Honolulu, Hawaii, USA.
[3]Hawaii Institute of Geophysics and Planetology, School of Ocean and Earth Science and Technology, University of Hawaii, Honolulu, Hawaii, USA.
[4]Department of Geology, Tulane University, New Orleans, Louisiana, USA.
[5]Now at Geophysical Institute, University of Alaska Fairbanks, Fairbanks, Alaska, USA.

0148-0227/03/2002JB001830$09.00

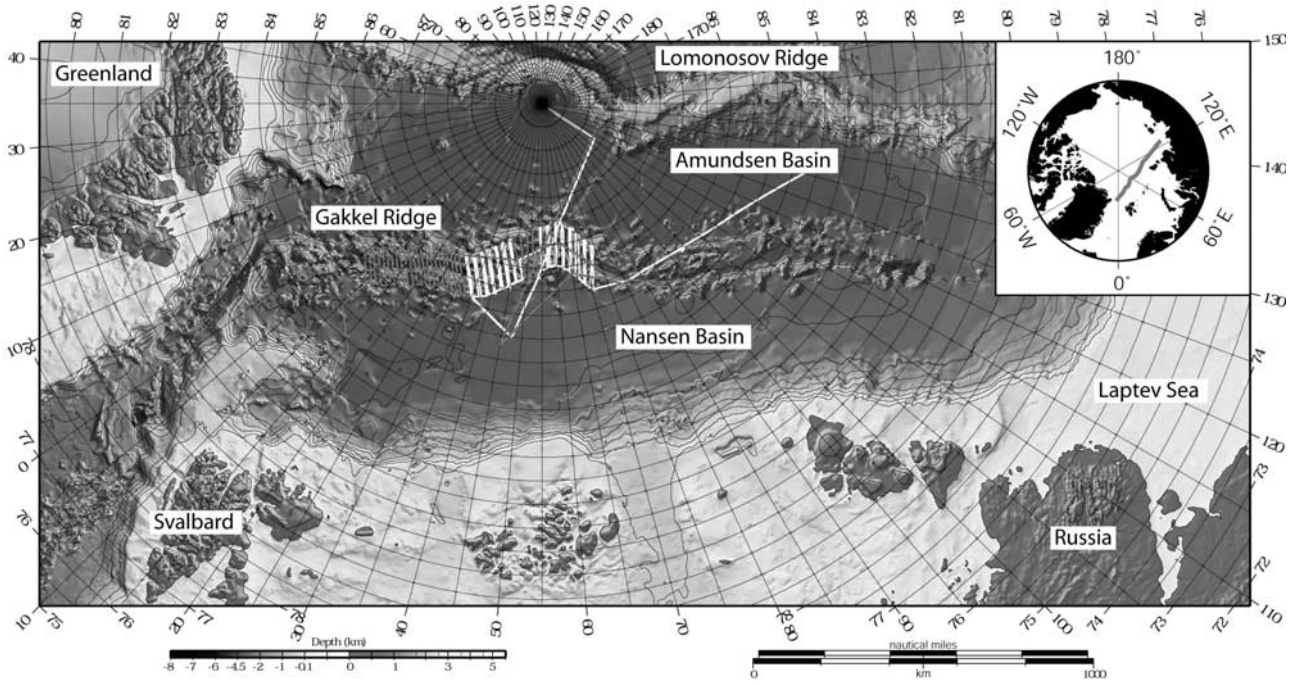

Figure 1. Bathymetric map of the Eurasian Basin showing the location of the Gakkel Ridge and tracks of the USS *Hawkbill* cruises, which collected the data on which this report is based. The 1998 cruise is shown in white and the 1999 cruise in red. Bathymetry is from the International Bathymetric Chart of the Arctic (IBCAO) database [*Jakobsson et al.*, 2000]. The inset shows the location of the Gakkel Ridge within the entire Arctic Ocean. See color version of this figure at back of this issue.

interpreted as a seafloor spreading anomaly sequence extending from anomaly 24 (~55 Ma) to the present [*Ostenso and Wold*, 1973; *Vogt et al.*, 1979; *Kovacs et al.*, 1985]. Total spreading rates determined from the magnetic anomalies have been less than 15 mm/yr throughout the opening of the Eurasian Basin. Current total spreading rates of 9–13 mm/yr are calculated for the western half of the basin, based on the distance from the axis to anomaly 5 (~10

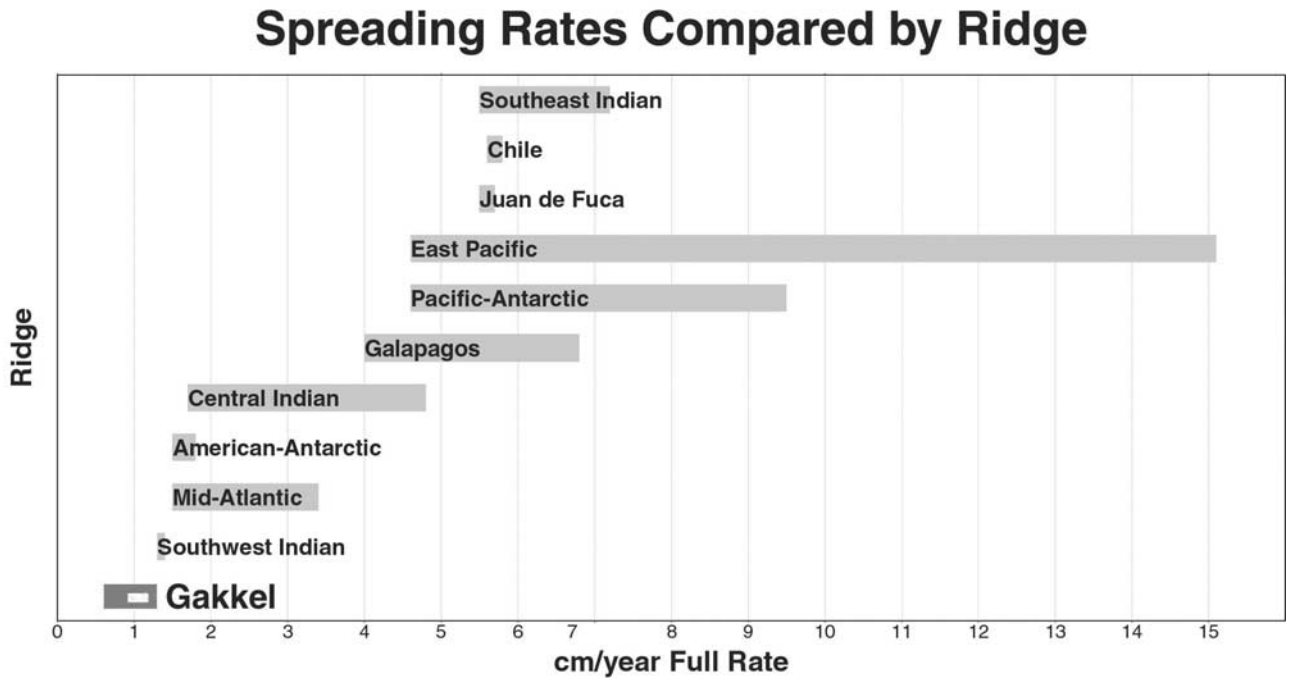

Figure 2. Spreading rates of different portions of the global mid-ocean system [*DeMets et al.*, 1994]. The white line within the Gakkel Ridge bar shows the range of spreading rates within our study area.

Ma), the youngest identifiable Chron [*Vogt et al.*, 1979] The NUVEL-1A global solution [*DeMets et al.*, 1994] gives present-day total opening rates that decrease from 12.7 mm/yr at the western end of the ridge to 6.0 mm/yr near the Laptev shelf, consistent with the magnetic data. For comparison, spreading rates observed on the Southwest Indian Ridge (SWIR) are in the range of 14–18 mm/yr (Figure 2) [e.g., *Bergh and Norton*, 1976; *Fisher and Sclater*, 1983; *Patriat*, 1987; *Rommevaux-Jestin et al.*, 1996].

[3] The morphology and petrology of mid-ocean ridges has been widely interpreted as controlled primarily by spreading rate. The extremely slow average spreading rate and the gradient in spreading rate along the Gakkel Ridge make the ridge an important end-member constraining models of mantle melting and crustal generation. Compilations of oceanic crustal thickness measurements [*Chen*, 1992; *White et al.*, 1992] have found a nearly constant average thickness of about 6–7 km for spreading rates from 20 to 150 mm/yr, implying a balance between melt production and spreading rate. This observation is consistent with melting models based on decompression melting of mantle that is upwelling in response to corner flow driven by plate separation [*Reid and Jackson*, 1981; *Bown and White*, 1994]. These models also predict that melt production and crustal thickness should decrease significantly at spreading rates less than about 15–20 mm/yr as the result of conductive cooling of the uprising mantle. The low spreading rate and range of spreading rates observed at the Gakkel Ridge provide an opportunity to test and calibrate these models.

[4] Extension at mid-ocean ridges involves both magmatic and mechanical extension. The balance and interplay between these two mechanisms of accommodating plate separation varies as a function of spreading rate to produce the differing ridge axis and flank morphology characteristic of fast spreading and slow spreading mid-ocean ridges [e.g., *Chen and Morgan*, 1990; *Mutter and Karson*, 1992; *Phipps Morgan and Chen*, 1993; *Carbotte and Macdonald*, 1994a, 1994b; *Tucholke and Lin*, 1994; *Macdonald et al.*, 1996; *Blackman et al.*, 1998]. Thus, the exceptionally slow spreading rate of the Gakkel Ridge may affect not only crustal thickness but also the form and along-axis distribution of volcanism and faulting, as well as the shape of the abyssal hills and the ridge segmentation.

2. Structure of the Eurasian Basin

[5] The continental Lomonosov Ridge divides the Arctic Ocean into two large oceanic basins, the Mesozoic-aged Amerasian Basin on the Pacific side and the Eurasian Basin on the Atlantic side. Aeromagnetic anomalies constrain the Eurasian Basin to have developed since the Early Cenozoic by seafloor spreading centered at the Gakkel Ridge [*Ostenso and Wold*, 1973; *Vogt et al.*, 1979; *Kovacs et al.*, 1985]. The oldest magnetic anomaly identified in the Eurasian Basin is anomaly 24 [*Vogt et al.*, 1979], so organized seafloor spreading on the Gakkel Ridge began at approximately the same time as farther south in the Norwegian–Greenland Sea and on the northern Reykjanes Ridge.

[6] Magnetic anomalies in the Eurasian Basin are generally linear and continuous. *Vogt et al.* [1979] state that "minor irregularities" in the anomaly pattern suggest the presence of several small (5–15 km) offsets and *Johnson et al.* [1990] argue for the presence of at least two fracture zone troughs between 55°E and 80°E to serve as conduits for sediments observed in the rift valley on some profiles across the eastern portion of the ridge.

[7] The Gakkel Ridge axis conforms to the shape of the conjugate margins, the Lomonosov Ridge and the Barents Shelf, suggesting that its geometry is inherited from the rifting event. The aeromagnetic data indicate that a 150 km right-stepping offset of the axis east of 62°E is the only ridge offset greater than about 15 km. *Cochran and Coakley* [1998] pointed out that the 62°E ridge offset is quite oblique to the local spreading direction and can not be a simple transform fault. The 62°E offset in the ridge axis maps back along a flow line to an offset in the Lomonosov Ridge near the North Pole and to an offset in the Eurasian continental margin at 60°–65°E (Figure 1). The 62°E offset appears to have been a persistent feature of the Gakkel Ridge since the initial rifting, and has been the only significant offset of the ridge axis throughout the development of the basin.

[8] Although the plate kinematic framework and spreading geometry of the Gakkel Ridge are reasonably well constrained from aeromagnetic studies [*Ostenso and Wold*, 1973; *Vogt et al.*, 1979; *Kovacs et al.*, 1985], the morphology and structure of the ridge are less well understood, largely because surface ships cannot easily operate in the area due to permanent pack ice. About 20 bathymetric profiles across the axis obtained from nuclear submarines have been published [*Johnson and Heezen*, 1967; *Johnson*, 1969; *Feden et al.*, 1979; *Vogt et al.*, 1979; *Coakley and Cochran*, 1998]. Almost all of these profiles are located west of 20°E at the western, fastest spreading end of the ridge. The only published multibeam bathymetry from the Gakkel Ridge are two Hydrosweep lines across the axis near 0°E and 56°E [*Jokat et al.*, 1995].

[9] Seismic refraction measurements in the Eurasian Basin are limited to the western portion of the basin to the west of 20°E [*Jackson et al.*, 1990; *Kristoffersen*, 1990] and show a great range of crustal thickness. Measurements in some regions give a normal oceanic crustal thickness of 6–8 km, while other measurements suggest very thin 2–3 km thick crust [*Duckworth et al.*, 1982; *Jackson et al.*, 1982]. *Jackson et al.* [1982] argue that, on a set of refraction lines collected on the ice station FRAM I, thicker crust is associated with unusually high amplitude seafloor spreading magnetic anomalies and thin crust with areas of lower amplitude magnetic anomalies.

[10] The region of high amplitude magnetic anomalies is referred to as the "Yermak H-Zone" by *Feden et al.* [1979] and extends from the Spitzbergen transform near 8°W to about 3°E. They attribute the high amplitude anomalies to the presence of fractionated, Fe-enriched and Ti-enriched basalt associated with the "Yermak hot spot" which also produced the paired Yermak and Morris Jessup plateaus near the Spitzbergen and Greenland margins. *Vogt et al.* [1979] noted that bathymetric profiles through areas with a high amplitude axial magnetic anomaly consistently have significantly shallower axial depths (3500–4000 m) than do profiles crossing the axis in regions with lower amplitude magnetic anomalies. The rift valley floor in regions of lower amplitude anomalies (which is most of the length of the ridge) is at 4700–5300 m depth. The axis of the Gakkel Ridge is the deepest bathymetric feature in the Arctic Ocean.

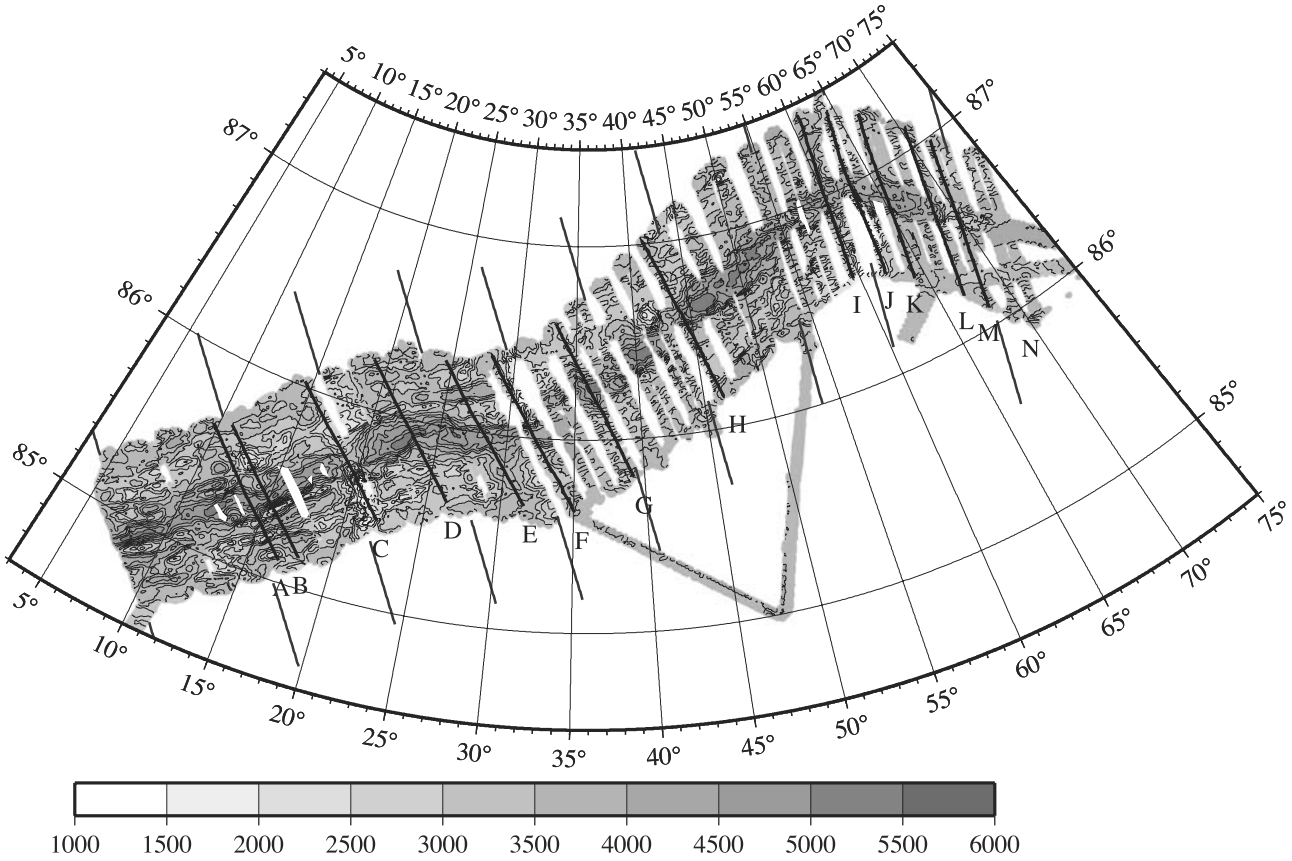

Figure 3. Bathymetry map of the western Gakkel Ridge based on gridded SCAMP bathymetry data obtained by USS *Hawkbill* during the 1998 and 1999 SCICEX cruises. Contour interval is 250 m with color changes at 500 m intervals. The location of the ridge axis is shown by a bold line. Solid lines outside the mapped area are parallel to the spreading direction. Solid lines on the map show ship tracks for profiles shown in Figure 6. Letters next to tracks correspond to those in Figure 6.

Rift valley relief was observed to remain relatively constant at 1400–2000 m in the two regions [*Vogt et al.*, 1979].

3. New Bathymetry and Gravity Data From the Gakkel Ridge

[11] Since 1993, the U.S. Navy has made a series of unclassified nuclear submarine cruises to the Arctic for scientific research through the Science Ice Exercises (SCICEX) program. Three of these cruises have conducted surveys of portions of the Gakkel Ridge. In 1996, the USS *Pogy* carried out surveys of four areas on the Gakkel Ridge, each consisting of five 80–90 km long lines spaced 15–20 km apart. Geophysical instrumentation on that cruise was limited to a narrow beam echo sounder and a Bell BGM-3 gravimeter [*Bell and Watts*, 1986]. *Coakley and Cochran* [1998] used the gravity and bathymetry data from the 1996 cruise to argue that the average crustal thickness is less than 4 km at the western Gakkel Ridge and may be ''vanishingly thin'' at the extremely slow spreading eastern portion of the ridge.

[12] The data presented and discussed in this paper were acquired by USS *Hawkbill* utilizing the Seafloor Characterization and Mapping Pods (SCAMP) geophysical instrument package which was installed for the 1998 and 1999 cruises. SCAMP consists of two sonar systems, a BGM-3 marine gravity meter [*Bell and Watts*, 1986] and a data acquisition system that logs the data and provides onboard quality control [*Chayes et al.*, 1996, 1999]. One of the sonar systems is a bilateral interferometric swath mapper that produces coregistered bathymetry and side scan image data. The second sonar system is a ''chirp'' (swept frequency) subbottom profiler. The transducer arrays are installed in pods mounted along the keel of the submarine. A hole was cut in the nonpressure hull above each pod to allow cables to be routed through the ballast tanks. The inboard electronics, gravimeter, and data acquisition system were installed in the torpedo room.

[13] The phase array sonar frequency is ~12 kHz, with a backscatter (side scan) swath width of ~160° and a bathymetric swath width of ~140°. In water depths are in excess of 1000 m the side scan swath width is ~20 km with bathymetric data out to ~10 km. Spatial resolution of the SCAMP system varies as a function of altitude off-bottom, survey speed, and sample position relative to the sub (nadir). Typically, surveys were conducted at 16 knots cruising at 750 feet (229 m) depth. Water depths along the Gakkel Ridge range from 600 to 5300 m. Spatial resolution for bathymetric data from the Gakkel Ridge survey averages 100–150 m across track with an along track sample interval of 99 m at 16 knots. Final bathymetric data has been gridded with 100 m^2 grid cells.

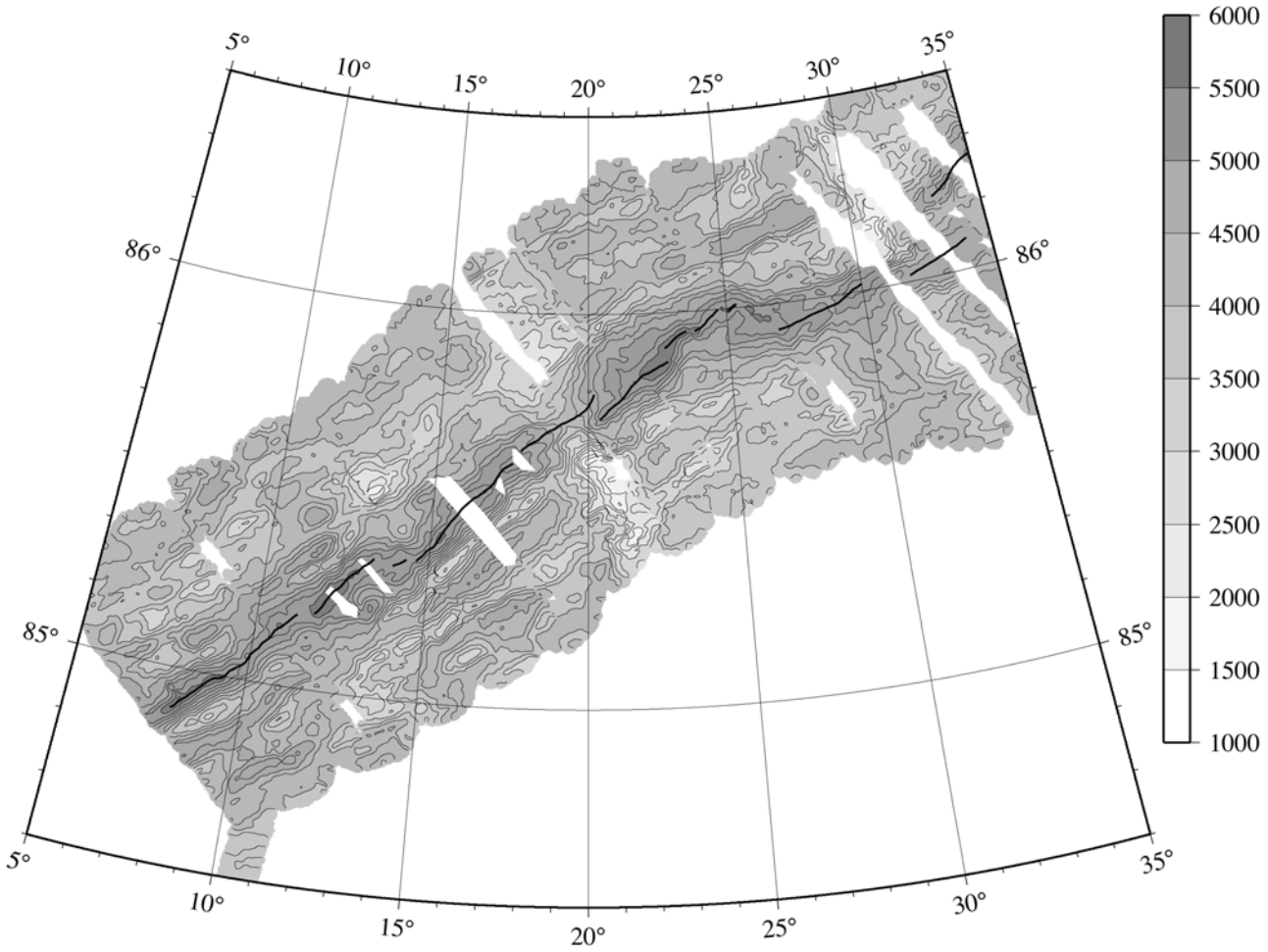

Figure 4a. Bathymetry map of the Gakkel Ridge from 5°E to 35°E based on gridded SCAMP bathymetry data obtained by USS *Hawkbill* during the 1998 and 1999 SCICEX cruises. Contour interval is 250 m with color changes at 500 m intervals. The bold line shows the location of the ridge axis.

[14] Under-ice navigation utilized the Navy's Submarine Inertial Navigation System (SINS), supplemented with occasional GPS fixes when the USS *Hawkbill* surfaced. The navigation was adjusted on a line-by-line basis through comparison of crossing lines and adjacent tracks to produce an internally consistent data set. Comparison by *Kurras et al.* [2001] of SCICEX navigation with GPS-navigated swath bathymetry from the Gakkel Ridge acquired in 2001 by USCGC Healy shows absolute positional accuracy of 3 km, with relative positioning estimated at better than 500 m.

3.1. Bathymetry Data

[15] The 1998 and 1999 cruises mapped the Gakkel Ridge axis for 850 km from 8°E to 98°E, obtaining nearly complete bathymetric and side scan data to about 50 km from the axis on both flanks from 8°E to 73°E and two swaths (total width of over 20 km) along the axis from 73°E to 98°E (Figure 1). Bathymetry maps of the Gakkel Ridge from 5°E to 75°E, the area in which cross-axis profiles were obtained, based on the Hawkbill bathymetry data, are shown in Figures 3 and 4. A side scan mosaic is shown in Figure 5.

[16] The rift valley is continuous throughout the surveyed region with no transform offsets. The prominent ridge offset east of 62°E is accomplished by a combination of non-transform offsets and oblique spreading (Figures 3 and 4c). The rift valley is 15–30 km wide and is 1200–2000 m deeper than the surrounding rift flanks throughout most of the area (Figures 4 and 6). The ridge axis location shown in Figures 3 and 4 was picked at intervals of 0.1° of longitude (<1 km) from detailed maps contoured at 10 or 20 m intervals. An along-axis depth profile is shown in Figure 7.

[17] The only location where the ridge axis is marked by a volcanic ridge on the rift valley floor, as is commonly the case on the Mid-Atlantic Ridge (MAR) [e.g., *Smith and Cann*, 1992; *Sempere et al.*, 1993; *Smith et al.*, 1995], is for ~25 km from 17.8°E to 20.2°E on the upper portion of an exceptionally shallow portion of the rift valley (Figure 4a). Throughout the rest of surveyed area, the axis is located within a valley. The valley floor varies from V-shaped to a flat 10 km wide flat surface, but is usually less than 5 km wide. Minor discontinuities offset the axis by 1.5–13 km. Figure 8 shows a bathymetry map of an ~45 km length of the ridge axis centered near 13°E, contoured at 25 m intervals. The lines nearly perpendicular to the axis in Figure 8 are

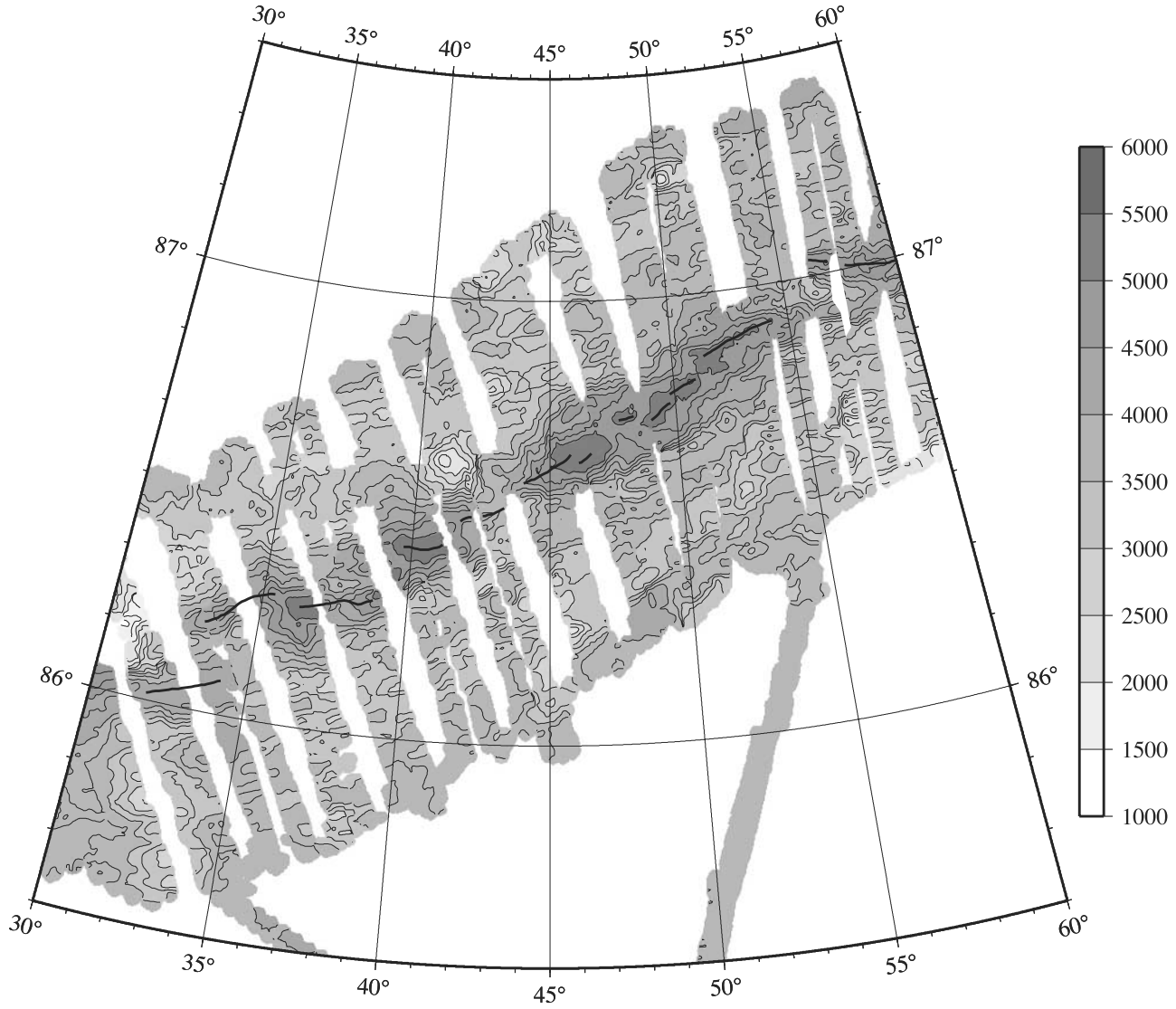

Figure 4b. Bathymetry map of the Gakkel Ridge from 30°E to 60°E based on gridded SCAMP bathymetry data obtained by USS *Hawkbill* during the 1998 and 1999 SCICEX cruises. Contour interval is 250 m with color changes at 500 m intervals. The bold line shows the location of the ridge axis.

seafloor spreading flowlines determined from the NUVEL-1A pole [*DeMets et al.*, 1994]. The ridge axis in this region consists of a number of short segments separated by oblique nontransform discontinuities (third-order discontinuities according to the classification of *Sempere et al.* [1993]).

3.2. Gravity Data

[18] Free-water gravity anomalies over the Gakkel Ridge from 5°E to 75°E, based on data collected on USS *Hawkbill* during the 1998 and 1999 SCICEX cruises, are shown in Figure 9. A free-water anomaly is equivalent to a free-air anomaly except that it takes into account the gravitational effect of the water above the measurement position as well as the free-air correction for the distance from sea level at which the measurement is made.

[19] The free-water anomalies resemble a low-pass filtered version of the morphology (Figure 6). The ridge axis is associated with a continuous large negative gravity anomaly. Local gravity maxima occur over the shallowest portions of the flanking rift mountains. The anomalies over the rift valley generally have a peak to trough amplitude of 85–150 mGal which, as pointed out by *Coakley and Cochran* [1998], is approximately 1.5–2 times that found on the MAR.

[20] Since free-air (or in our case, free-water) gravity anomalies are dominated by the gravitational effects of the large density contrast at the seafloor and thus appear as a ''low-pass filtered'' version of the morphology, it has become common to remove the gravity effects of the crust–water interface in order to reveal more subtle density variations masked by the large gravity effects of seafloor relief. In fact, the common practice is not to just remove the gravity effects of the bathymetry, which results in a Bouguer anomaly, but also the gravity effect of the crust–mantle boundary assuming a constant thickness crust [e.g., *Prince and Forsyth*, 1988; *Kuo and Forsyth*, 1988; *Lin et al.*, 1990; *Pariso et al.*, 1995; *Detrick et al.*, 1995]. The resulting ''mantle Bouguer'' anomalies (MBAs) are interpreted as

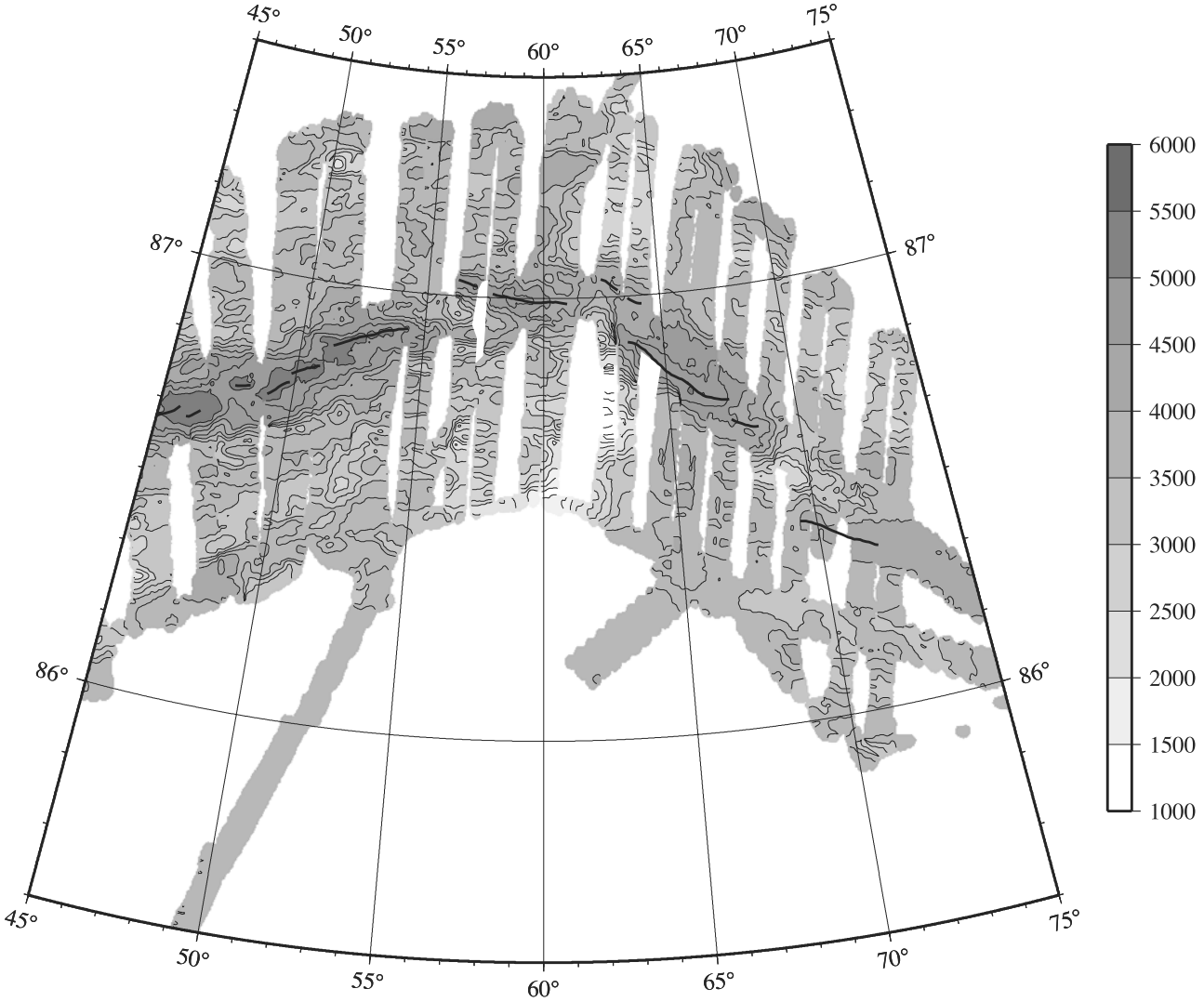

Figure 4c. Bathymetry map of the Gakkel Ridge from 55°E to 75°E based on gridded SCAMP bathymetry data obtained by USS *Hawkbill* during the 1998 and 1999 SCICEX cruises. Contour interval is 250 m with color changes at 500 m intervals. The bold line shows the location of the ridge axis.

resulting from some combination of lateral variations in crustal thickness, crustal density, and mantle density.

[21] We calculated the mantle Bouguer correction following the method developed by *Prince and Forsyth* [1988] and *Kuo and Forsyth* [1988] except that, following the conclusions of *Coakley and Cochran* [1998], we assumed a 2 km rather than the a 6 km crustal thickness. The gravity effects of crustal and mantle relief were calculated using four terms in the *Parker* [1973] method of calculating the gravity effect of relief on interfaces. Density contrasts of 1700 and 600 kg/m^3 across the water/crust and crust/mantle boundaries were assumed. We sampled the grids of water/crust and crust/mantle gravity effects at the locations of the free-water gravity measurements, subtracted these values point-by-point from the free-water anomalies and gridded the point MBAs in the same manner as was done with the point free-water anomalies to produce the MBAs shown in Figure 10. An along-axis profile is shown in Figure 7. The MBA in the western survey area, where the bathymetric coverage is more complete and the gravity lines regularly spaced, are smoother than in the east where data gaps and uneven line spacing have introduced local variations. We also calculated MBAs assuming a 6 km crust to determine the effect of the difference in our assumption of a thin crust from the conventional assumption of a 6 km crust. Although the amplitudes of maxima and minima varied, the pattern of anomalies is identical and our conclusions would not have been altered by assuming a 6 km crust.

[22] Often, variations in mantle density due to temperature variations away from a spreading center are modeled assuming a passive flow model [*Phipps Morgan and Forsyth*, 1988] with the appropriate spreading rate and ridge axis geometry, and their gravity effect removed from MBAs to produce a residual MBA (RMBA). *Coakley and Cochran* [1998] calculated the gravity effect of mantle density variations resulting from seafloor spreading and the resulting upwelling and spreading at the very low spreading rates of the Gakkel Ridge using the technique of *Phipps Morgan and Forsyth* [1988]. They found that, due to the very slow upwelling rate at Gakkel Ridge spreading rates and the

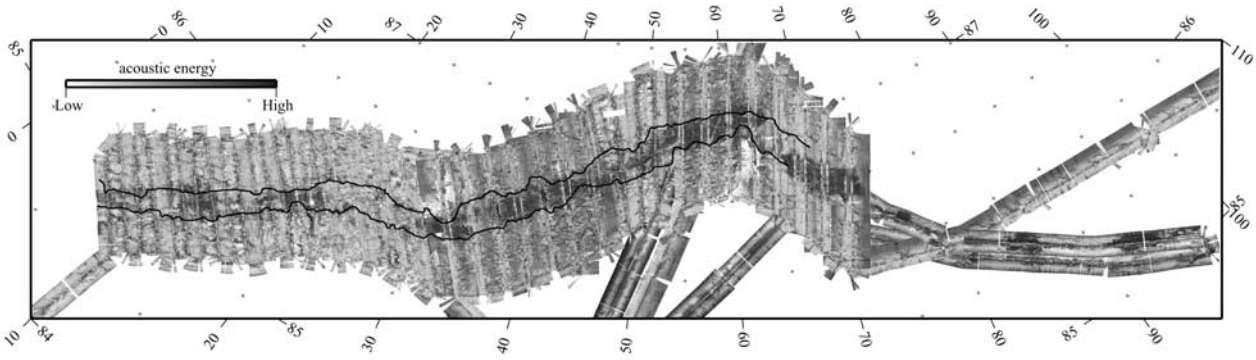

Figure 5. Side scan map of the Gakkel Ridge from 5°E to 98°E based on SCAMP side scan data obtained by USS *Hawkbill* during the 1998 and 1999 SCICEX cruises. Black represents very high energy returns and white represents very low energy returns.

resultant conductive cooling, the mantle thermal contribution to the MBAs is less than 3–4 mGal over the ~50 km (8–10 Ma) extent of our data away form the axis. We have therefore chosen not to apply a thermal correction to our data. It is this conductive cooling during the slow upwelling that led to the prediction that melt production is severely retarded at Gakkel Ridge spreading rates [*Reid and Jackson*, 1981; *Bown and White*, 1994].

[23] MBAs have been commonly interpreted in terms of crustal thickness variations although the few available comparisons of gravity and seismic measurements show that crustal density variations can be significant particularly near transform ridge offsets [*Tolstoy et al.*, 1993; *Minshull*, 1996; *Hooft et al.*, 2000]. This difference has been interpreted as due to fracturing and alteration of both crust and mantle near transform segment boundaries resulting in lower densities [*Hooft et al.*, 2000]. We calculated the variations in crustal thickness that could result in the observed MBA by downward continuation of the gravity anomalies from the sea surface to a depth of 5.740 km (the 3.740 km average water depth plus the assumed 2 km crustal thickness). Since downward continuation is unstable at short wavelengths, we first applied a low-pass filter to the gravity data that removed all wavelengths less than 30 km and passed wavelengths greater than 40 km. The downward continued gravity anomalies were converted to an equivalent mass layer and relief on that surface determined assuming a density contrast of 600 kg/m^3 across the Moho. A map of the calculated crustal thickness variations is shown in Figure 11. The crustal thickness shows significant variations (>4 km) within our survey area.

4. Axis-Perpendicular Ridges

[24] Three highstanding bathymetric ridges oriented perpendicular to the ridge axis at 19°E, 32°E, and 63°E are a prominent feature of the Gakkel Ridge (Figures 3 and 4). The axis-perpendicular ridge at 19°E intersects the ridge axis at its shoalest point within the survey area. The ridge axis reaches 3500 m near 19°E, 1500 m shallower than adjacent portions of the axis (Figure 7). The 19°E axis-perpendicular ridge coincides with a 40–50 mGal mantle Bouguer gravity low (Figures 7 and 10) which may imply up to 3 km of crustal thickening under the 19°E axis-perpendicular ridge (Figure 11).

[25] Side scan and bathymetry data show multiple flow fronts and small volcanic features within the rift valley near 19°E in contrast to the rest of the surveyed ridge axis [*Kurras et al.*, 1999]. This is also the only place in the surveyed portion of the Gakkel Ridge where an axial volcanic ridge is observed. Off-axis portions of the 19°E axis-perpendicular ridge show several rounded bathymetric highs indicative of volcanic construction. However, these off-axis features show low acoustic reflectivity (Figure 5), probably due to sediment cover, suggesting that the igneous activity that created the ridge has occurred at the axis. The bathymetric ridge and MBA gravity lows extend to the boundaries of our survey area, implying that this has been the site of exceptionally vigorous magmatic activity and the production of thicker crust since at least 8.3 Ma.

[26] The axis-perpendicular ridges at 32°E and 63°E are similar to each other, but differ significantly from the 19°E ridge. The ridge axis at both 32°E and 63°E is 4100–4200 m deep, which is 600 m deeper than at 19°E, although shallower than in much of the surrounding rift valley. Side scan data show high reflectivity in the rift valley at both 32°E and 63°E (Figure 5), suggesting the presence of flows near the axis at both locations. However, the axis is marked by a valley rather than the volcanic ridge observed at 19°E and the large number and variety of volcanic features observed along the axis near 19°E are not observed at these locations. The flows on the rift valley floor near 32°E and 63°E appear to have originated at isolated central volcanoes (Figure 4b).

[27] The ridge flank bathymetry at both 32°E and 63°E is asymmetric (Figures 4, 6f, and 6j). The ridge flank rises abruptly on one side of the axis to form ~15 km wide, very shallow linear bathymetric ridges that extend away from the axis parallel to the spreading direction (Figure 4). Minimum depths reach ~1350 m on the northern 32°E ridge and ~600 m on the southern 63°E ridge. The ridge at 63°E, which has been given the name Langseth Ridge in honor of the late Dr. Marcus Langseth, is the shallowest known bathymetric feature within the Eurasian Basin. These large ridges are not associated with significant MBA gravity lows (Figure 10) and are not areas of thickened crust. They thus appear to be tectonic rather than volcanic in origin. A similar morphology and structure is associated with the distinctive inside corner features observed adjacent to transforms and at some smaller nontransform offsets on the

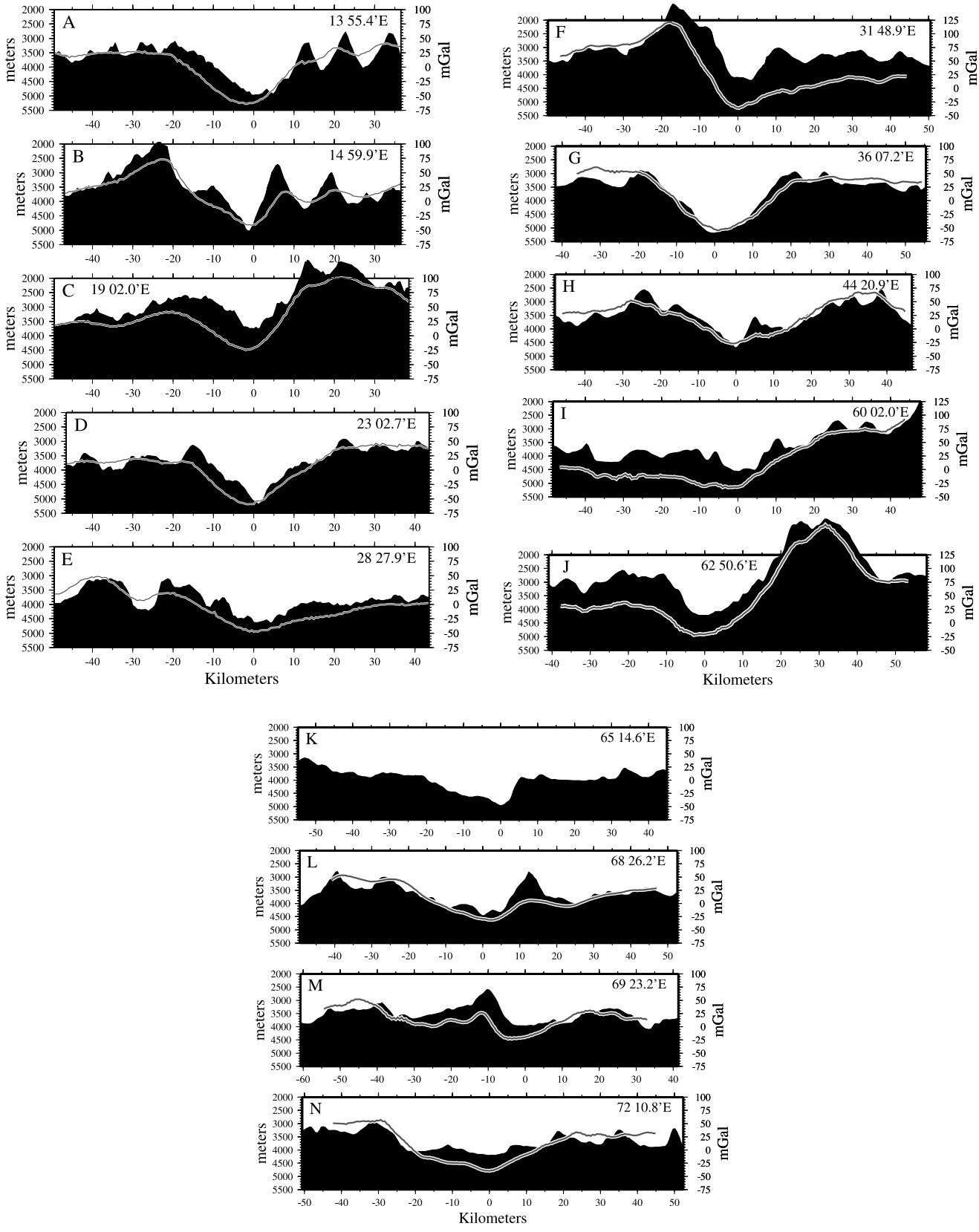

Figure 6. Selected bathymetry and free-water gravity profiles across the Gakkel Ridge. Profiles are projected along the local spreading direction with the axis as the origin. North is to the left (negative distances). The longitude at which each profile crosses the axis is noted. Letters on each profile correspond to those on Figure 3, which shows the locations of the profiles.

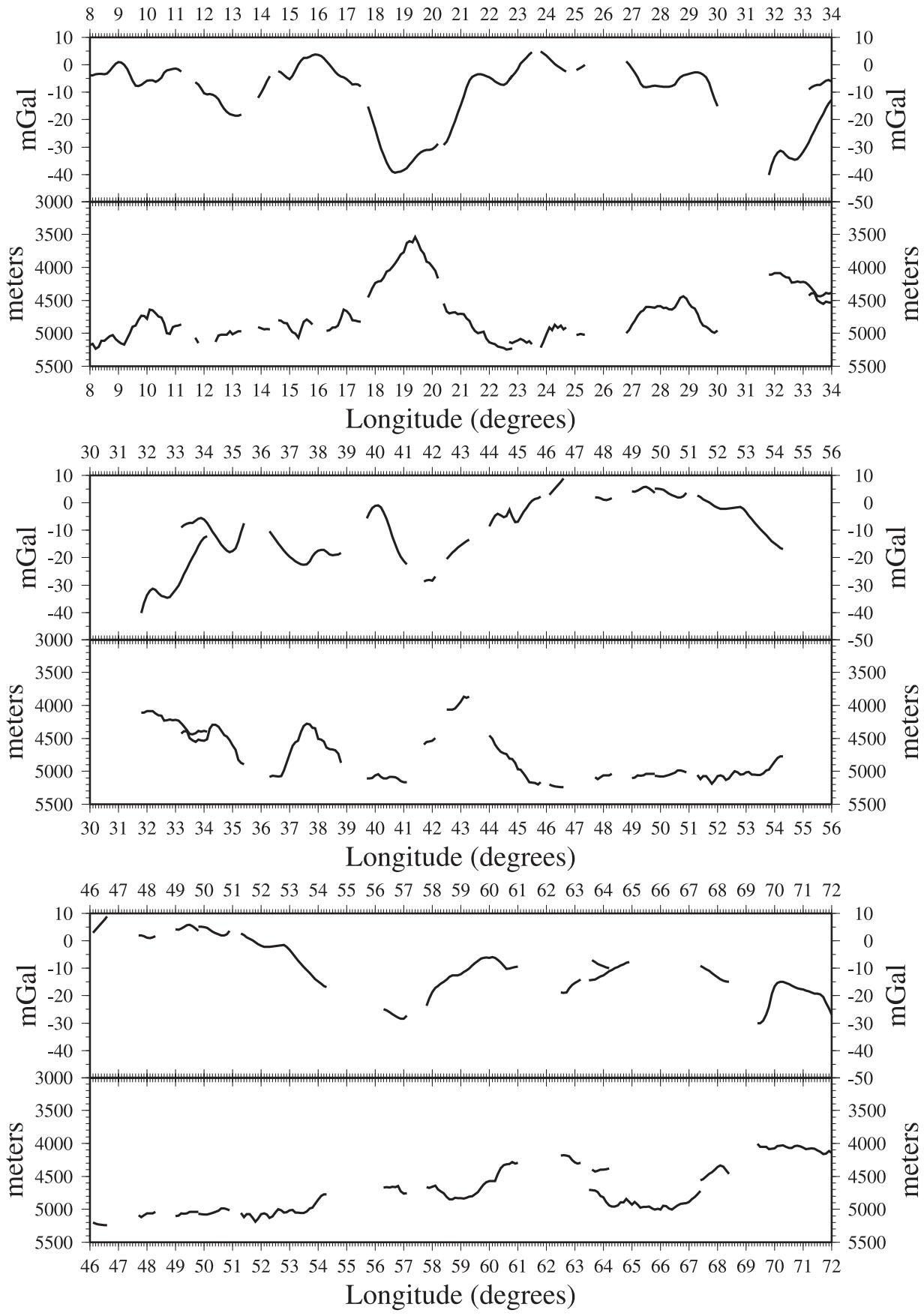

Figure 7. Variations in axial depth and axial mantle Bouguer gravity anomaly along the Gakkel Ridge. Depth is at the bottom and gravity at the top in each panel.

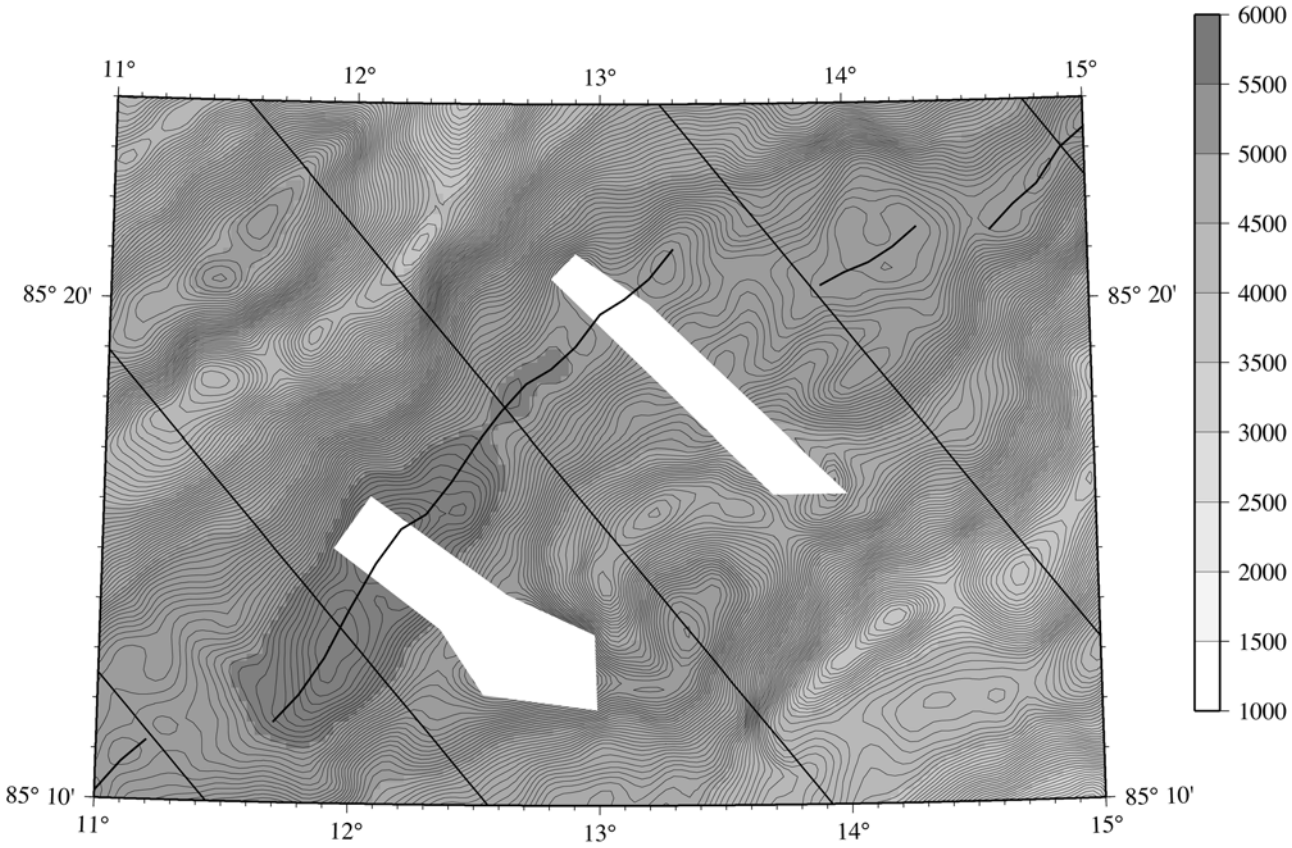

Figure 8. Bathymetry map of the Gakkel Ridge axis from 11°E to 15°E contoured at 25 m intervals. Bold line shows location of the ridge axis. Solid lines running roughly NW-SE are parallel to the spreading direction. Note that the axis is consistently located at the bottom of a valley and that the axis consists of a series of segments nearly orthogonal to the spreading direction connected by oblique accommodation zones. See color version of this figure at back of this issue.

MAR [e.g., *Severinghaus and Macdonald*, 1988; *Blackman and Forsyth*, 1991; *Mutter and Karson*, 1992; *Tucholke and Lin*, 1994].

[28] The Gakkel Ridge rift valley is continuous with no transform offsets throughout the mapped region, so the axis-perpendicular ridges at 32°E and 63°E are not associated with offsets of the axis. However, the two ridges are located at distinct changes in the trend and obliquity of the Gakkel Ridge (Figure 3). From the western limit of our data at ~8° to 25.5°E, the ridge axis has a consistent linear trend of N60°E. From 33°E to about 55°E, the axis has an overall trend of N50°E, while from 63°E to 80°E the axis has an overall trend of about N140°E. There is another change in the strike of the ridge near 80°E. East of 80°E, the axis has a consistent trend of about N125°E to the easternmost USS *Pogy* line at 101°E. We have insufficient off-axis data to determine whether an axis-perpendicular ridge is present on the northern ridge flank at 80°E.

5. Western Section (West of 32°E)

[29] The ridge axis in the western section is uniformly very deep, in the range of 4500–5250 m (Figure 7). The deep axial valley appears to extend about 50 km beyond our survey area to 3°E where *Dick et al.* [2001] report a nearly 1000 m decrease in average axial depth to the west. Near 19°E, the axis shallows to 3500 m at the location of the shallow axis-perpendicular ridge. This shallow region does not result from a systematic shoaling of the axis toward the center of a segment, as normally observed at the MAR [e.g., *Sempere et al.*, 1990, 1993; *Lin et al.*, 1990; *Detrick et al.*, 1995]. Rather the axis shallows very rapidly by 1200–1600 m within a distance of about 20 km approaching 19°E from each direction. The ridge axis is deeper than 4500 m throughout the rest of the ~250 km mapped length of the western section with no systematic pattern of along-axis depth variation.

[30] Minimum depths in the rift mountains throughout most of the western section are in the range of 2700–3300 m, so the rift valley relief is generally 1500–2200 m (Figures 4a and 6a–6e). The rift flanks in the western portion of the ridge section consist of a series of large linear ridges separated by deep valleys that often reach depths of over 4000 m (Figures 4a, 6a, and 6b). The scarps bounding these large blocks often appear to be formed by a single fault scarp, particularly between 13°E and 19°E on the south flank. The 9 km compound ridge offset at 13.5°–14.5°E (Figure 8) corresponds to a change in the character of the northern flank from linear ridges toward the west to a more massive morphology in the east. However, on the

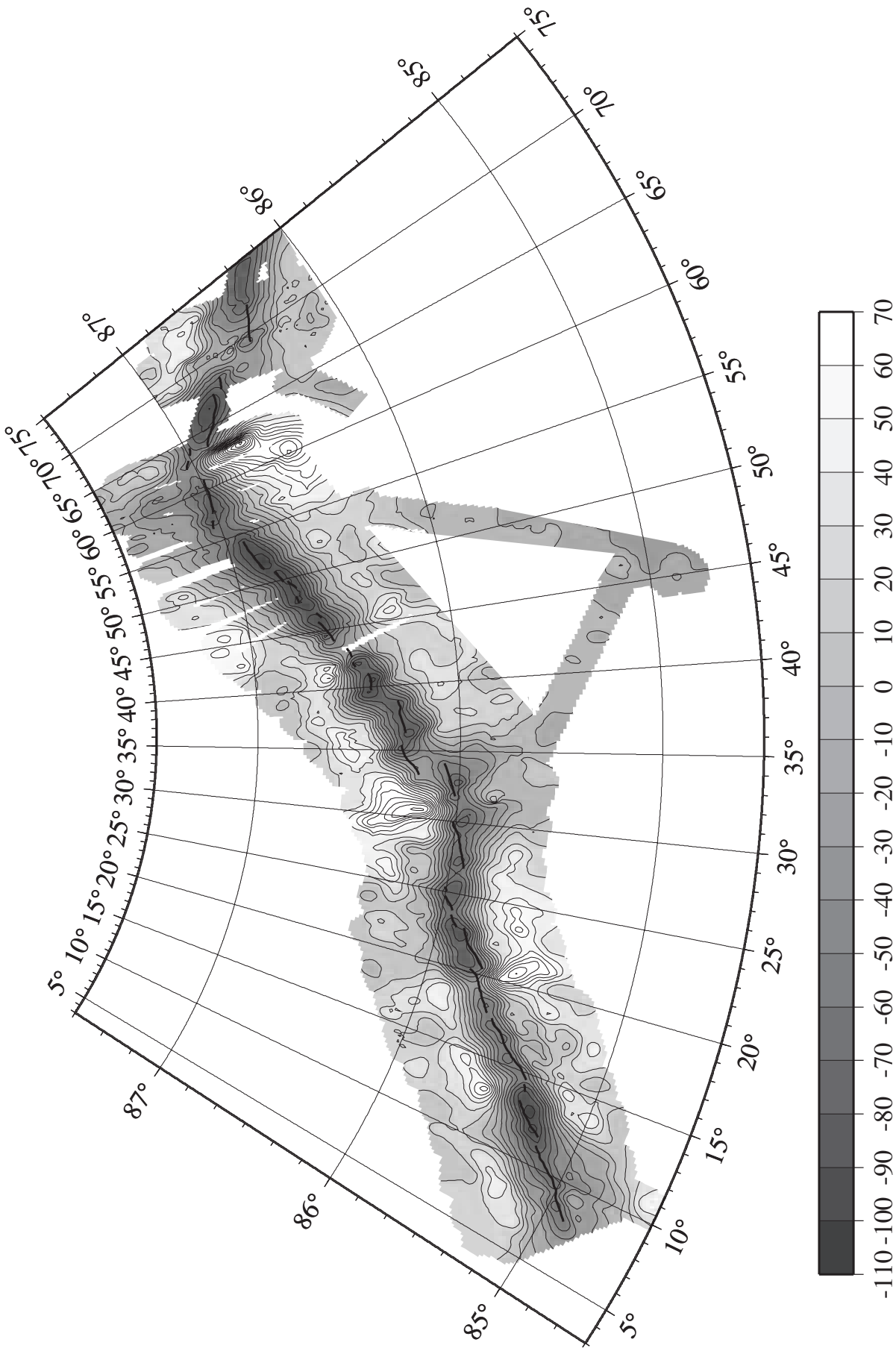

Figure 9. Free-water gravity anomalies over the Gakkel Ridge based on data acquired by USS *Hawkbill* during the 1998 and 1999 SCICEX cruises. Contour interval is 10 mGal. The bold line shows the location of the ridge axis.

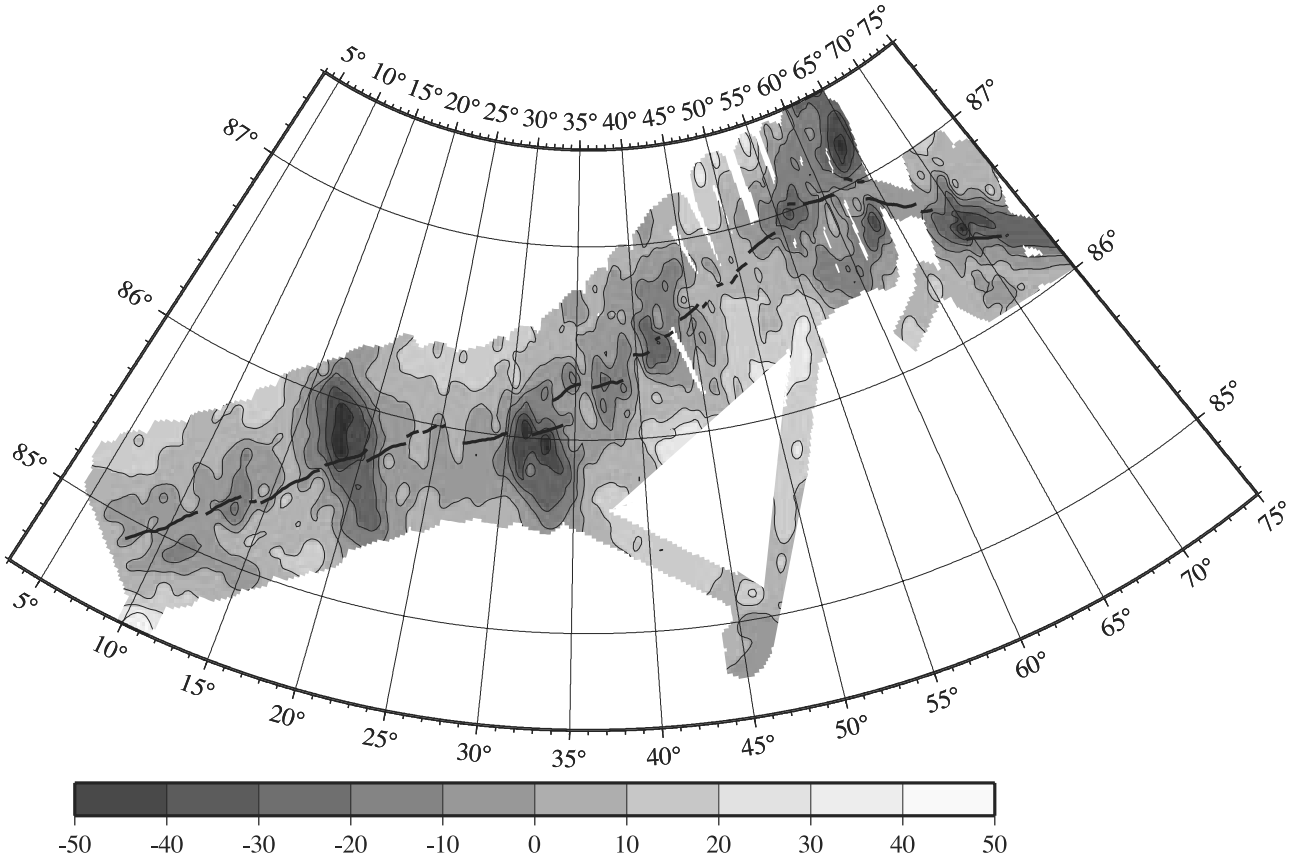

Figure 10. MBAs over the Gakkel Ridge based on data acquired by USS *Hawkbill* during the 1998 and 1999 SCICEX cruises. The MBA were calculated assuming a 2 km mean crustal thickness [*Jackson et al.*, 1982; *Coakley and Cochran*, 1998] and density contrasts of 1700 and 600 kg/m^3 at the water/crust and crust/mantle interfaces. Contour interval is 10 mGal. The bold line shows the location of the ridge axis.

south flank, there is no indication of the presence of a ridge offset and the large linear ridges making up the ridge flank are continuous across the offset. The bathymetric pattern changes to the east of the 19°E axial high. Here there are still linear rift-parallel ridges, but they are superimposed on plateaus found on both flanks at a depth of 3000–3500 m (Figure 6d) instead of being separated by deep fault-bounded troughs. Approaching the eastern end of the section, the ridges on the southern flank die out and the plateau deepens to 3800–4000 m with subdued relief (Figures 4a and 6e). In contrast, on the northern flank, relief on the ridges increases approaching the large "inside corner" ridge at 32°E.

[31] There is very little evidence of magmatic activity in the western section other than near 19°E. There are no volcanic landforms or areas of high reflectivity east of the 19°E axis-perpendicular ridge. Other than the 19°E complex, the only clear site of volcanic activity, either at the axis or on the ridge flanks, in this section of the ridge is at 13°–14°E where two large rounded bathymetric highs are located on the north flank of the rift valley along a flow line crossing the axis at a relatively shallow (~4700 m) location near 14.6°E (Figures 4a and 7). We interpret these features as volcanoes based on their morphology. The larger volcano, which has a diameter of 12–15 km and reaches a depth of 1900 m, is located 23 km (3.9 Ma) from the axis just outside the rift valley. The second volcano, which reaches a depth of 3300 m is located 10 km (1.7 Ma) from the axis on a ledge on the northern rift valley wall. (Figures 4a and 6b). Side scan data indicates that the volcano 23 km from the axis is sediment covered while the smaller one, 10 km from the axis, is highly reflective (Figure 5). An acoustically reflective region in the axial valley floor near 13°E appears to result from flows erupted from this volcano.

[32] The volcanoes on the north flank of the rift valley at 14.6°E appear to be point-source magmatic centers locally piling magma on top of the crust slightly to the north of the ridge axis rather than axial magmatic centers accommodating significant extension. This is suggested by the observations that there is no morphology suggestive of volcanic activity at the ridge axis (Figure 8) and that the southern flank of the rift valley to the west of the 19°E bathymetric high consists of a series of large, narrow, elongated, fault-bounded ridges which appear to be entirely tectonic in origin (Figures 4a and 6b).

[33] With the exception of the 13 km offset near 26°E, all of the ridge offsets are less than 5.5 km. A 9 km offset at 13°–14.5°E is accommodated by two oblique offsets separated by a 4 km long ridge-parallel basin (Figure 8). Ridge

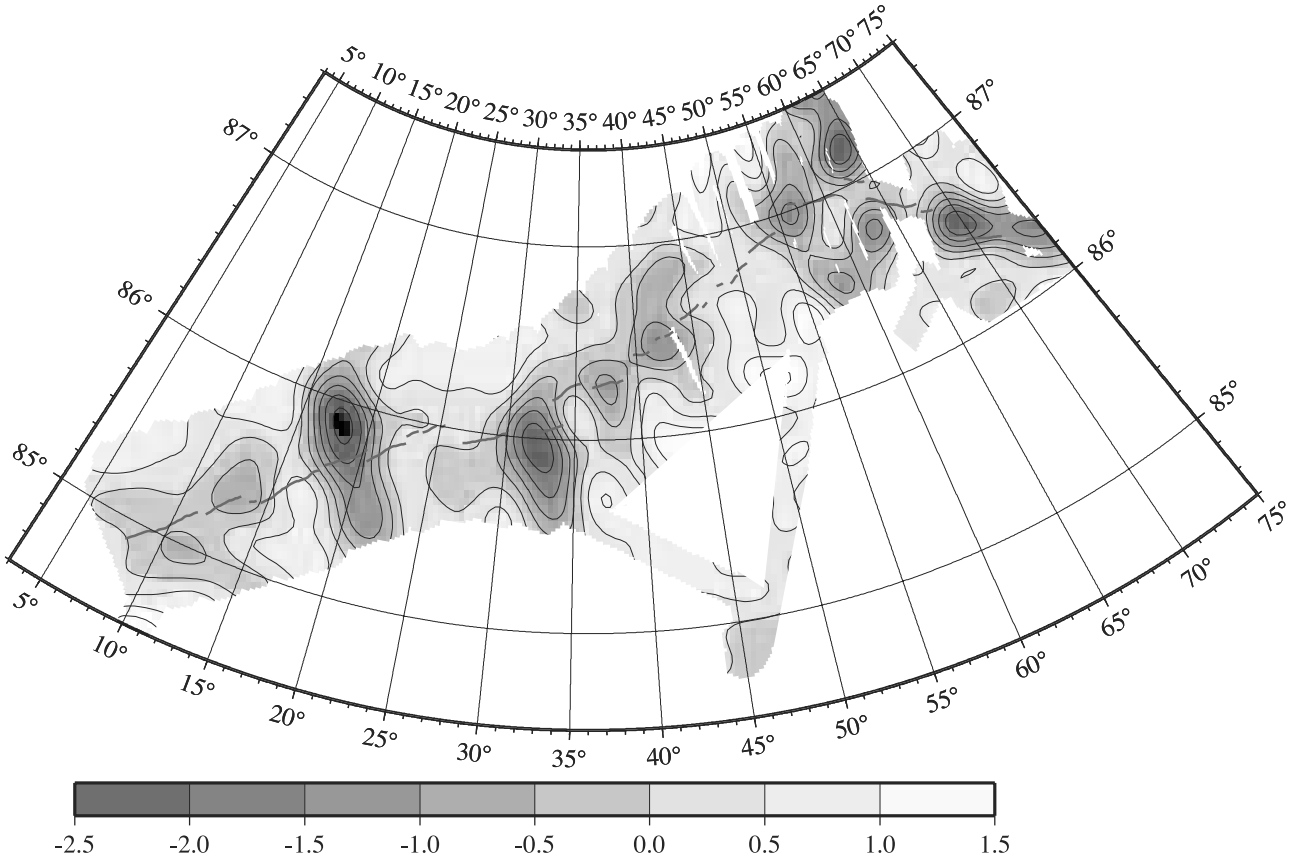

Figure 11. Relative crustal thickness variations calculated by downward continuation of the MBAs (Figure 10). Contour interval is 0.5 km. Negative values denote thicker crust. The bold line shows the location of the ridge axis.

offsets are generally accommodated by oblique valleys oriented at 40°–60° to the spreading direction. The 26°E offset trends about N130°E, which is only 23.5° from the local spreading direction (N153.5°E) and is the closest to a transform offset observed along the Gakkel Ridge.

6. Central Section (32°–63°E)

[34] The ~235 km long 32°–63°E section trends about 20° from perpendicular to the spreading direction. Locally, the ridge axis trends roughly perpendicular to the local spreading direction and is offset to the north by a series of nontransform discontinuities of 1.5–14 km offset to create the overall oblique trend of the ridge. The ridge offsets are located in oblique valleys. All but two of them offset the axis by less than 8 km. The ridge axis is generally deep, at a depth of 5000–5250 m and is characterized by a valley throughout this portion of the ridge. The deepest point in the Arctic Ocean appears to be located at the ridge axis near 47°E.

[35] There are three local axial bathymetric highs reaching shallower than 4500 m centered near 37.5°E, 43.5°E, and 55.5°E (Figures 4b and 4c). Axial depths shallower than 4500 m are also found from 31°E to 35°E and from 60°E to 64°E in the vicinity of the 32°E and 63°E axis-perpendicular ridges (Figures 4b and 7). Evidence of volcanic activity in the form of individual central volcanoes is found on each of the areas of shallower ridge axis, and much of the rift valley floor in this section of ridge shows high acoustic reflectivity that appears to result from relatively recent flows emanating from these central volcanoes.

[36] The 43.5°E axial bathymetric high, in which the rift valley floor shoals to a depth of 3850 m, is the only portion of the axis other than the 19°E high in which the axis shoals to less than 4000 m. However, this high differs from the 19°E high in that the axis is marked by a valley, it lacks the abundant small-scale volcanic features observed near 19°E, and there is no axis-perpendicular ridge. This area has been the site of significant but episodic volcanism, as shown by the presence of several volcanoes on the ridge flanks. A large volcano, which reaches a depth of 2000 m is located atop the north wall of the rift near 86°38′N, 41°E. A smaller volcano is located about 20 km to the NNE at 86°48.N, 42.8°E. On the south flank, a possible volcanic feature is present about 40 km from the axis at 86°16′N, 45.7°E (Figure 4b).

[37] The volcanoes observed at 56°E and at 33°–35°E, just east of the 32°E ridge, appear to be intimately related to the two largest ridge axis discontinuities in this section of the ridge, a 13 km offset near 34°E and a 14 km offset at 55°–56°E. These two ridge offsets are unusual because the two ridge segments are separated by a bathymetric high (the volcano) with no obvious connection between the two rift tips. Part of the ridge between the two rift tips at the 34°E offset occurs in a data gap between two swaths (Figure 4b),

so it is possible that an accommodation zone exists in that gap. However, at 55°–56°E, it is clear that there is not a bathymetric connection between the two ridge tips (Figure 12). It is possible that the 55°–56°E offset actually occurs in two steps and that the volcano was formed at and completely overprints a short stretch of extensional ridge axis located between the two visible rift tips as part of a compound offset such as observed near 14°E (Figure 8).

[38] The volcanoes observed at 37.5°E and 60°E are relatively small features perched several hundred meters above the ridge axis on the first fault ledge above the rift valley. The 60°E volcano can be seen near 87°02.5′N, 60°E in Figure 12. It is a small circular cone about 2.5 km in diameter and 300 m high. In spite of its small size, flows from this volcano spread for more than 10 km both east along the ledge and south and east along the axis. The perched volcano located north of the axis at 37°E is somewhat larger, roughly 2 × 6 km, but is also about 300 m high. Side scan data again imply that flows from this volcano spread for more than 10 km along the axis (Figure 5).

[39] The small 60°E volcano has no expression in either the free-water or MBA gravity anomalies. The other volcanoes in the central ridge section are associated with local MBA gravity lows. However, none of these gravity anomalies approach either the amplitude or geographical extent of the MBA lows at 19°E or at the 32°E and 63°E "outside corners." The largest MBA low both spatially and in amplitude (∼20–25 mGal) is located at 43°E. This MBA gravity low is centered over the ridge axis and the large volcano atop the north wall of the rift valley at 41°E. The gravity low extends with a reduced amplitude to another apparently volcanic bathymetric high centered at 86°50′N, 43°E (Figures 4b and 12). The other MBA lows at 34°E, 37.5°E, and 56°E have amplitudes of 10–20 mGal but are very closely confined to the area of the volcanic edifice.

[40] The ridge flanks in the central section to the west of the 43.5°E bathymetric high are similar to those observed in the eastern portion of the western (8°–32°E) ridge section. They consist of a plateau at a fairly constant depth of 3000–3500 m on which a series of ridges with relief of up to about 700 m high superimposed (Figures 4b and 6g). East of 45°E, the rift flank plateau deepens to 3500–3800 m. East of about 54°E, as the 63°E ridge is approached, the north flank deepens further to almost 4000 m with more subdued relief. The southern flank on the other hand, begins to shallow as it approaches the Langseth Ridge inside corner massif (Figure 6i). The shoaling is observed east of 55°E at the southern end of our data 30–50 km from the axis and becomes closer to the axis as the Langseth Ridge is approached.

7. Eastern Sections (East of 63°E)

[41] The ∼175 km stretch of ridge axis between 63°E and 80°E is highly oblique to the spreading direction. The ridge trends roughly N140°E, 25°–40° from perpendicular to the spreading direction (Figure 3). The ridge axis from 63°E to 67°E is deep (4800–5000 m) (Figures 4c and 7) and is located near the southern edge of a 1000 m deep, 20 km wide valley (Figures 4c and 6k). The southern boundary of the valley is very steep, while the valley floor slopes up gradually to the north. The seafloor outside the rift valley is nearly flat at a depth of about 4000 m. There are basically no rift mountains flanking the ridge axis in this area (Figures 4c and 6k), particularly on the southern flank. East of about 69°E, rift mountains reaching depths of 3200–3700 m are observed (Figure 6n).

[42] The ridge axis can be traced east to about 86°41′N, 68.5°E immediately to the north of a large bathymetric ridge that reaches a depth of 2600 m (Figures 4c, 6l, and 13). The western tip of the next section of ridge axis can be identified near 86°27′N, 69°24′E (Figures 4c, 6m, and 13), ∼18 km to the south. The ridge between the two rift tips can be identified as a volcano based both on morphology and the presence of high acoustic reflectivity areas, interpreted as flows, surrounding it (Figure 5). The 69°E ridge offset is thus similar to the offset at 56°E.

[43] East of the large volcano at 69°, the ridge axis is located within a few hundred meter deep, flat valley which appears to be largely filled with sediments (Figures 4c, 6n, and 13). The shallow axial valley extends at a fairly constant depth of 4000–4500 to the eastern end of our data at 98°E. *Coakley and Cochran* [1998] discuss a set of bathymetry and gravity profiles across the axis across the Gakkel Ridge at 94°E to 102°E and conclude from the gravity data that a deep rift valley is present, but is nearly buried by sediments.

[44] Our across-axis lines extend only as far east as about 72°E. East of 72°E, we have only two bathymetry swaths parallel to the axis which provide information on the valley floor, south wall and southern ridge flank near the axis (Figure 1). The rift valley east of 72°E generally consists of a relatively flat valley at a depth of 4200–4600 m that is bounded by steep, 300–600 m high walls. We do not have adequate bathymetry data to determine whether the change in trend at 80°E is accompanied by distinctive bathymetry as observed at 32°E and 63°E (Figure 13).

[45] *Edwards et al.* [2001] interpret SCAMP bathymetry and side scan data from the lines along the axis east of 80°E. Their data shows two areas of high reflectivity located near 85°E and 93°E (Figure 5) corresponding to topographic highs with 500 to 1000 m relief, protruding through the sediments in the rift valley. They interpret these bathymetric features as young volcanoes. The relationship between areas of high acoustic return and tectonic lineations observable in the side scan data led *Edwards et al.* [2001] to conclude that the two volcanoes have been recently active. This conclusion is supported for the volcano at 85°E by an earthquake swarm lasting through much of 1999 at the location of the volcano in which the seismic records exhibit a volcanic character [*Müller and Jokat*, 2000; *Tolstoy et al.*, 2001]. *Edwards et al.* [2001] conclude that volcanic activity at the extremely low spreading rates of the Gakkel Ridge east of 80°E may consist of reasonably voluminous, sustained eruptions focused at a few discrete sites.

[46] At both sites where *Edwards et al.* [2001] identified volcanoes with associated young flows within the rift valley, less acoustically reflective volcanic landforms are also observed on the southern rift flank about 10 km south of the axial volcanoes. This suggests that these specific locations have the site of repeated episodes of voluminous sustained volcanic activity over at least the past 2 Ma. Away from these discrete volcanoes, the rift flanks reach a depth of about 3800 m, barely above the 4000 m depth of

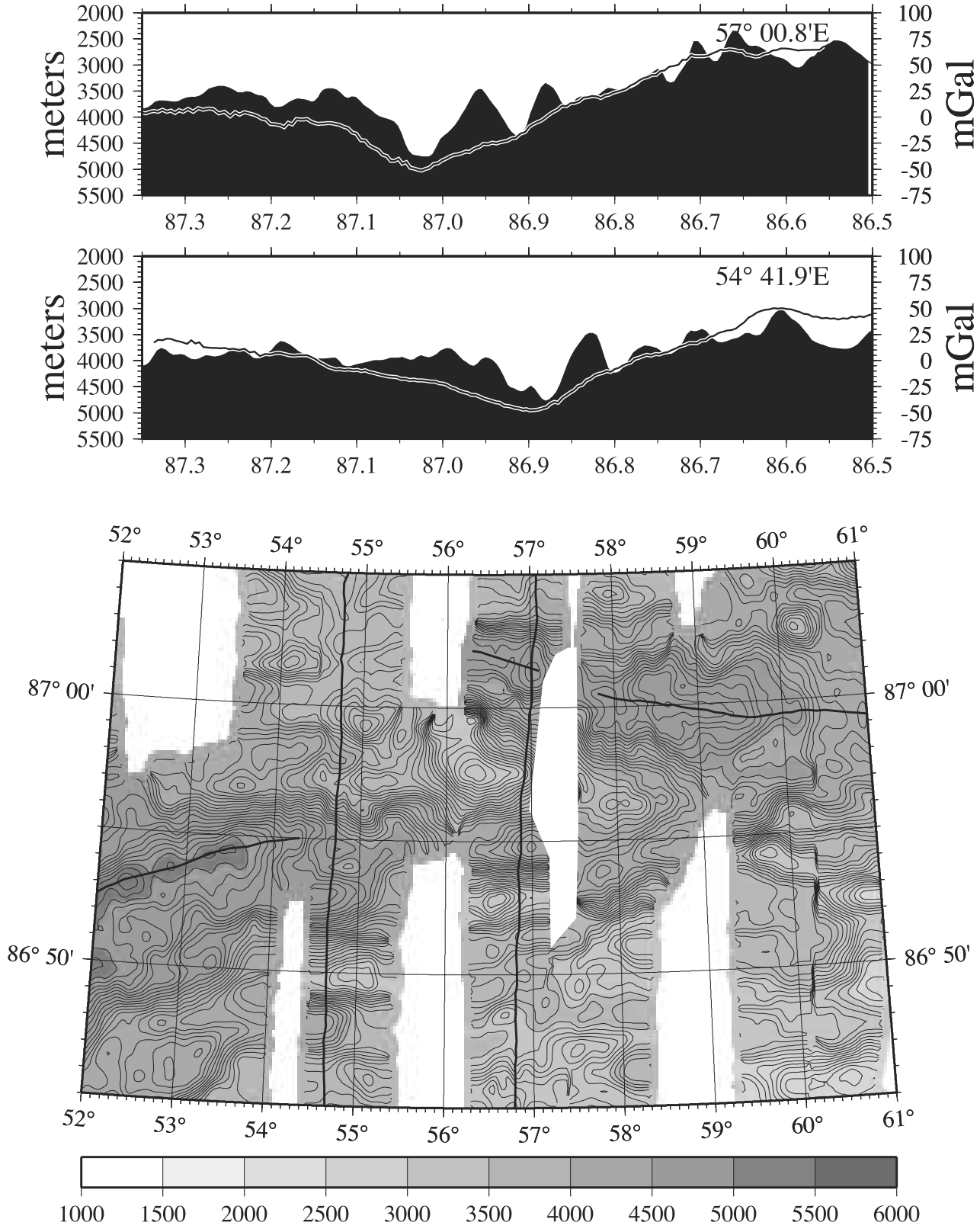

Figure 12. (bottom) Bathymetry map of the Gakkel Ridge axis from 52°E to 61°E based on gridded SCAMP bathymetry data. Contour interval is 50 m with color changes at 500 m intervals. The bold line shows the location of the ridge axis. The location of two bathymetry and free-water gravity anomaly profiles (top) plotted against latitude is also shown on the map. The ridge axis is offset to the north by 14 km between 55°E and 56°E as is clearly demonstrated by the two bathymetric and gravity profiles. There is no bathymetric evidence of a shear zone between the two rift tips. The region of the offset is occupied by a bathymetric high, which appears to be of volcanic origin based on bathymetry and side scan data.

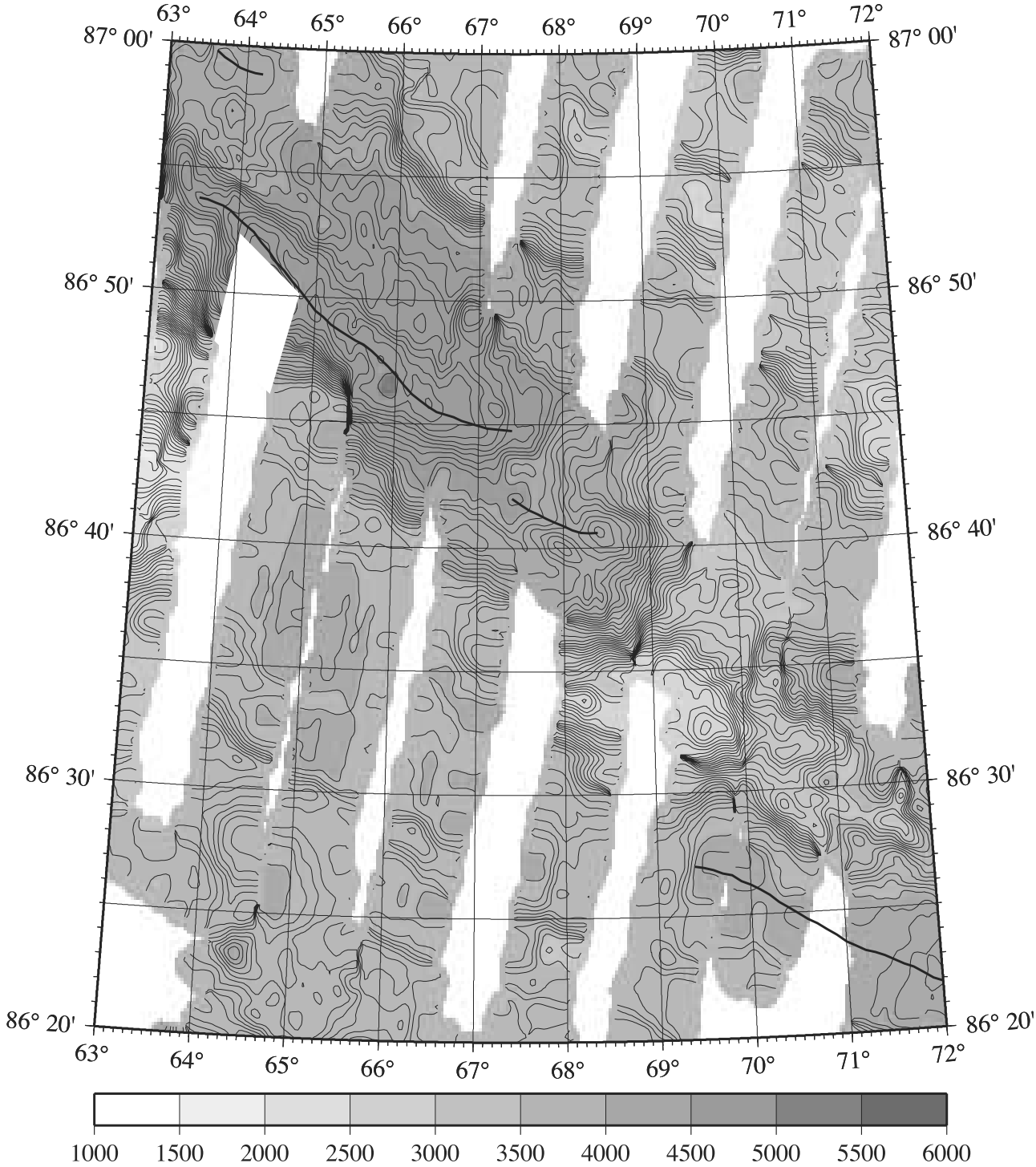

Figure 13. Bathymetry map of the Gakkel Ridge axis from 63°E to 72°E based on gridded SCAMP bathymetry data. Contour interval is 50 m with color changes at 500 m intervals. The bold line shows the location of the ridge axis. The spreading axis steps 18 km to the south near 69°E. The area between the rift tips is occupied by a large bathymetric high, apparently of volcanic origin.

the flanking abyssal plains [*Coakley and Cochran*, 1998; *Edwards et al.*, 2001].

8. Discussion

[47] The Gakkel Ridge between 5°E and 65°E, spreading at a total rate of 10.5–12.1 mm/yr, appears on first glance to be similar in structure to the more accessible, well-studied MAR, where the spreading rate is 2–4 times as higher. Specifically, the ridge axis is located within a 15–20 km wide, 1–2 km deep rift valley flanked by rugged, fault-bounded rift mountains. The axis of the Gakkel Ridge and the MAR are also both marked by a large negative free-air gravity anomaly with gravity highs over the rift mountains.

However, the similarities in the morphology of the Gakkel Ridge and the MAR are in many ways superficial. The structure and segmentation of the Gakkel Ridge differ from those of the MAR in a number of significant respects that appear to result from differences in the crustal accretion process at the extremely slow spreading rate of the Gakkel Ridge.

[48] The most obvious difference is melt production and crustal thickness. Melting models based on decompression melting of upwelling mantle [e.g., *Reid and Jackson*, 1981; *Bown and White*, 1994; *Sparks and Parmentier*, 1994] predict that melt production and crustal thickness decrease rapidly at spreading rates less than about 15 mm/yr as the result of conductive cooling of the uprising mantle. The few seismic studies that exist away from the "Yermak H-Zone" to the west of 3°E have consistently shown thin 2–3 km crust [e.g., *Duckworth et al.*, 1982; *Jackson et al.*, 1982, 1990]. Quantitative modeling of bathymetry and gravity profiles across the Gakkel Ridge led *Coakley and Cochran* [1998] to conclude that if the average crustal density is less than 2900 kg/m^3, than the average crustal thickness must be less than 4 km and probably no more than 1–2 km to satisfy the gravity data.

[49] The extensive swath mapping and gravity surveys of the Gakkel Ridge carried out during the SCICEX98 and SCICEX99 cruises of USS *Hawkbill* provide evidence that the effects of the extremely slow spreading rate and resulting reduced melt supply are not restricted simply to the production of an unusually thin crust but that ridge segmentation and the crustal accretion process including the form and distribution of magmatism are also significantly different than at faster spreading ridges.

8.1. Crustal Accretion

[50] A major difference between the Gakkel Ridge and the MAR is that evidence of extrusive volcanism is confined to a limited number of specific locations on the Gakkel Ridge. Three types of volcanic features can be identified on the mapped portion of the Gakkel Ridge: (1) the 19°E volcanic system, which is an unique feature and which has created a highstanding band of thickened crust extending away from the ridge, (2) about 10 distinct volcanic constructs with a few hundred to 1500 m of relief distributed along the axial valley and near-axis regions, and (3) areas of high acoustic reflectivity interpreted as low relief flows. Small volcanic features, which are ubiquitous on the MAR [*Smith and Cann*, 1990, 1992, 1993], are not observed on the Gakkel Ridge in either the bathymetry with 10 m and 20 m contour data or in the side scan data, except near 19°E.

[51] The axial valley floor near 19°E is the site of numerous small-scale volcanic features that coalesce to form an axial volcanic ridge as well as being scattered about the valley floor. The valley floor is covered with acoustically reflective flows (Figure 5). The low reflectivity of the ridge flanks and lack of evidence of large-scale off-axis volcanism implies that the thickened crust extending away from the ridge at 19°E was created within the rift valley and subsequently transported up and out onto the ridge flanks. The 19°E volcanic system thus appears to be the only location in the surveyed portion of the Gakkel Ridge where ridge crest activity typical of the MAR axis is occurring. Since gravity data suggest that a several km thick crust is being created within the rift valley, it is likely that a crustal section typical of the MAR exists at 19°E, including gabbros, dikes, and the flows and small volcanoes visible at the surface.

[52] The vigorous axial magmatic center at 19°E contrasts greatly with the rest of the Gakkel Ridge west of 32°E. With the exception of the volcano on the north wall of the rift valley near 14°E and a flow on the valley floor that appears to have emitted from it (Figures 4a and 5), there is no evidence of any other volcanic activity for 225 km from 30°E to the western end of our data at 8°E (Figures 3 and 4a). The nonmagmatic portion of the ridge axis likely extends westward for another 50 km to 3°E [*Dick et al.*, 2001]. Other than near 19°E, the ridge axis is consistently marked by a valley rather than a volcanic ridge (Figure 8). It thus appears that, with the exception of a single off-axis volcano at 14°E, all extrusive volcanic activity for 275 km along the ridge occurs in a ~30 km stretch of the axis near 19°E, which is the most vigorous magmatic site in our survey area.

[53] The pattern of volcanism in the 32°–63°E section of ridge is very different than in the western section. The ridge axis shallows to less than 4500 m depth at five locations in the 235 km from 32°E to 63°E. Each of the shallow areas is associated with volcanism. In addition, much of the floor of the rift valley is covered with acoustically reflective material identified as volcanic flows (Figure 5). However, although volcanism is widespread, it is of a more surficial nature than at 19°E. The volcanoes are all well-defined isolated central volcanoes often located off-axis or on the rift valley walls, not magmatically active portions of ridge axis, as at 19°E. The ridge axis remains a valley near these isolated volcanoes without the small-scale volcanic features typical of ridge axis volcanism. It appears probable that the crust throughout much of the central section consists largely of extrusive basalt erupted directly over peridotite.

[54] There are local MBA gravity lows of 10–25 mGal over each of the individual volcanoes except for the small 60°E volcano (Figure 10). Although there are no bands of low gravity as at 19°E, the regions from 30°E to 45°E and from 55°E to 65°E have generally lower MBA gravity anomalies (Figure 10), both on-axis and off-axis, than does much of the western ridge section or the portion of the central section from 45°E to 55°E where the axis is very deep and there are no volcanoes. The gravity data may be interpreted as implying as much as 1 km thicker crust in these regions (Figure 11). It is possible that the episodic, localized volcanic activity and associated widespread flows have created a reasonably thick layer of basalt at the seafloor which is not present in areas such as 45°–55°E, 3°–13°E, or 22°–26°E where there is no evidence of volcanic activity. The seafloor in these nonvolcanic regions may be largely peridotite or covered with a thin veneer of basalt from flows along the axis.

[55] The greatly reduced amount of melt produced by decompression melting at extremely low spreading rates [*Reid and Jackson*, 1981; *Bown and White*, 1994; *Sparks and Parmentier*, 1994] is insufficient to maintain a magmatic spreading axis. Instead, melt that reaches the seafloor is erupted at a series of distinct locations along the axis. East of 32°E, multiple eruptions over time at these sites have built up isolated central volcanoes and covered adjacent

portions of the axial valley with low relief lava flows (Figures 4 and 5) [*Edwards et al.*, 2001]. These volcanoes are irregularly spaced at 25–95 km intervals along the axis between 32°E and 63°E. and east of 80°E. The large volcano at 69°E is the only volcanic landform within the 175 km section of ridge between 63°E and 80°E. However, three areas of high reflectivity, interpreted as lava flows, are spaced about 30 km apart within the sediment-filled rift valley between the 69°E volcano and the volcano at 85°E discussed by *Edwards et al.* [2001] (Figure 5). It thus appears that the limited amount of melt produced as the result of upwelling at these extremely slow spreading rates is focused to discrete eruption sites where repeated eruptions have built up volcanic edifices [*Edwards et al.*, 2001].

[56] The spreading rate decreases by only about 5.5% (11.59–10.95 mm/yr) between 19°E and 43.5°E and by 8.5% (to 10.60 mm/yr) from 19°E to 60°E. Barring a sudden "threshold effect" change in the upwelling pattern, spreading rate variation is therefore not likely to be the immediate cause of the difference between the region west of 32°E where volcanic activity is dominated by and concentrated at the large 19°E complex, and the ridge to the east of 32°E, where volcanism is distributed at a number of smaller volcanoes.

[57] It is more likely that the 19°E complex is the result of a localized source of melt. If so, it is in many ways an ultraslow spreading analog to the "Plume" segment at 33°S on the MAR, which has 1500 m of relief in axial depth and shows the largest observed "bulls-eye" MBA gravity low [*Kuo and Forsyth*, 1988; *Fox et al.*, 1991; *Tolstoy et al.*, 1993]. *Michael et al.* [1994] analyzed basalt samples from the 33°S and adjacent segments and concluded that the most likely reason for the thicker crust and shallow axial depths in the 33°S segment is interaction of the axis with a passively imbedded chemical inhomogeneity in the mantle. *Michael et al.* [1994] estimated that the increase in melt production was only 6–8%, but that early melting of the heterogeneity promotes focusing of the upwelling in the segment above the heterogeneity, leading to the large intra-segment variation in crustal thickness and axial depth observed at 33°S on the MAR. Analysis of recently obtained samples from the Gakkel Ridge [*Langmuir et al.*, 2001] is needed to determine whether such a mechanism can result in the nearly complete focusing of all volcanic activity in the 3°–32°E section of the Gakkel Ridge and the formation of the band of thick crust extending away from the axis at that location.

8.2. Segmentation

[58] The Gakkel Ridge axis is continuous without any transform offsets. However, sections of the ridge axis show distinctly different linear trends. Changes in ridge trend at 32°E and 63°E are associated with similar, very prominent bathymetric features that share a number of characteristics with each other and with inside/outside corner complexes observed at the MAR. We do not have the data to determine whether similar bathymetry exists at the 80°E change in ridge trend. The change in trend at 32°E is associated with a change in the style of volcanism. It is unclear that the changes in trend at 63°E and 80°E are expressed in the magmatic budget, although a single large central volcano at 69°E is located within the rift from 63°E to 80°E, rather than the smaller, more numerous volcanoes along the axis east of 80°E and west of 63°E. It is thus unclear whether the term "segment," which has come to imply interaction between surface features and magma supply, should be applied to these divisions of the ridge axis.

[59] The most obvious bathymetric features related to the changes in ridge strike are the large "inside corner" ridges. These consist of ~15 km wide ridges that rise abruptly from the rift valley floor at 4000–4200 m to reach depths of ~1340 m at 32°E and 600 m at 63°E. These ridges stretch away from the axis to at least 50 km off-axis (Figures 3 and 4). Directly opposite the inside corner highs at the Gakkel Ridge, there is an ~15 km wide stretch of rift flank with depths of 2700–3200 m which slopes down along-axis in both directions to an area of deep rift flanks where the minimum depths are only 3800–4000 m (Figures 4, 6e, and 6i). The juxtaposition of the highstanding ridge and the deep outside corner gives the ridge axis a characteristic asymmetric appearance.

[60] The free-water gravity anomalies exhibit very large positive values on the shallow ridge flank at both 32°E and 63°E (Figures 6f, 6j, and 11), as might be expected given the very large topographic relief. However, the MBAs on the shallow side of the axis do not show the presence of the highstanding ridges. This is particularly evident at 32°E where the gravity contours to the north of the axis are perpendicular to the bathymetric ridge (Figure 10). There is a small amplitude (~10 mGal) MBA low over the southern ridge at 63°E, but it is much less prominent than the low over the deeper northern flank. The localized MBA low at 86°45′N, 63°E is an artifact due to navigational errors in an area of very large depth and gravity gradients (Figure 4c). The gravity data therefore implies that the extremely shallow ridges to the north of the axis at 32°E and south of the axis at 63°E are not the sites of significant crustal thickening and thus appear to be of tectonic rather than volcanic origin. In fact, the crust appears to be significantly thicker on the opposite, deeper flanks, which are marked by MBA gravity lows. This asymmetry is in crustal thickness also characterizes MAR ridge discontinuities.

[61] The similarity in morphology and gravity anomalies at ridge discontinuities on the MAR and changes in the strike of the Gakkel Ridge raises the possibility that these inside/outside corner complexes arise from similar processes. Inside/outside corner complexes at the MAR are interpreted to result from the presence of a detachment fault dipping below the ridge axis from the inside corner toward the outside corner, so that the inside corner forms the footwall and the outside corner the hanging wall [e.g., *Brown and Karson*, 1988; *Mutter and Karson*, 1992; *Tucholke and Lin*, 1994]. The detachment is considered to bottom out in a zone of distributed shear below the brittle/ductile transition. According to this model, the upper crust is effectively stripped off of the inside corner, so that the remaining crust is both denser and thinner than normal oceanic crust resulting in the large positive MBA values observed at MAR. Since the crust is very thin or even patchy to start with at inside corners on the Gakkel Ridge, this mechanism will not be effective at the Gakkel Ridge. Therefore, the lack of an large "inside corner" gravity high is not surprising. The important comparison is that both on the MAR and the Gakkel Ridge, the highstanding "inside

corner'' ridge does not have thickened crust and is of tectonic origin.

[62] In *Tucholke and Lin*'s [1994] development of the detachment model, the detachment responsible for the inside corner complex extends from the ridge axis offset at the end of the segment either to the next ridge axis discontinuity or dies out near the segment center. It is perhaps possible that single detachment faults extend the length of the 3°–32°E and 32°–63°E sections of the Gakkel Ridge. However, at both 32°E and 63°E, the ridge axis steps toward the outside corner by 10–14 km along nontransform offsets approaching the bend from either direction (Figures 3 and 4). These nontransform offsets at 26°E and 34° and at 56°E and 64°E are among the largest observed offsets of the axis along the Gakkel Ridge. These nontransform ridge offsets bounding the portion of the axis interacting with the inside/outside corner complex may bound a shorter hypothesized detachment surface.

[63] One difficulty is to explain the presence of a large gravity low over the outside corner at the Gakkel Ridge. A simple explanation, applicable to the MAR, is that the upper crustal material removed from the inner corner making it thinner and denser ends up on the outer corner making it thicker and less dense. This does not apply at the Gakkel Ridge with its very thin crust. A second possibility is that the segment boundaries on the Gakkel Ridge are the sites of enhanced magmatic activity. However, there is no bathymetric evidence of enhanced volcanism on the outside corners.

[64] A third possibility is large-scale serpentinization and the presence of serpentine diapirs. The detachment fault could serve as an efficient conduit to introduce water relatively deep into the mantle resulting in extensive serpentinization. *Tucholke and Lin* [1994] hypothesize that intrusion of serpentinite diapirs is an important process during periods of amagmatic extension at MAR outer corners, citing the frequent occurrence of serpentinite from outer corner dredge halls and the well documented exposure of serpentinized ultramafic rocks at some outside corners.

[65] If there is a detachment fault dipping beneath the axis, then downward flexure of the hanging wall [*Weissel and Karner*, 1989] will contribute to the deep ridge flank and low gravity anomalies on the outside corner. Quantification of this effect depends on knowledge of the dip of the detachment and the thickness and rigidity of the lithosphere. However, given the thick lithosphere expected near the Gakkel Ridge, flexure could make a major contribution to the observed deep outer corner ridge flank and associated gravity low.

9. Summary and Conclusions

1. The supply of magma to the extremely slow spreading Gakkel Ridge is insufficient to maintain a continuous volcanic axis. Bathymetric evidence of extrusive volcanic activity is limited and confined to specific locations. The ridge axis is generally marked by a valley rather than a constructional axial volcanic ridge as commonly observed on the MAR. Ridge flank bathymetry is primarily tectonic in origin and is characterized by linear rift-parallel bathymetric ridges and fault-bounded troughs with up to 2km of relief on fault scarps.

2. East of 32°E, discrete central volcanoes are observed at 25–95 km intervals along the rift valley, often located off-axis in the rift valley or perched on the rift valley walls. The abundant small-scale volcanism characteristic of the MAR axial valley [*Smith and Cann*, 1990, 1993; *Smith et al.*, 1995] is not observed, although lava flows from the isolated volcanoes cover large areas of the axial valley floor. It appears that melt is delivered directly to the seafloor and erupted at a set of distinct locations where multiple eruptions have built up individual central volcanoes and covered adjacent areas with low relief lava flows. The crust in this area probably consists of basalt directly overlaying peridotite. Gravity data implies that up to 1 km of low density basaltic crust may be present in portions of Gakkel Ridge axis and flanks, but that there are also sizable areas where the seafloor consists mainly of peridotite.

3. West of 32°E to at least 8°E, and probably to 3°E, there is virtually no volcanic activity observed except at a ~30 km length of ridge axis centered near 19°E. At this location, the ridge axis abruptly shoals by 1500 m at the location of a highstanding ridge extending perpendicular to the axis for at least 50 km (8.3 Ma). Bathymetry and side scan data show the presence of numerous small volcanic features and multiple flow fronts in the axial valley on the upper portions of the 19°E along-axis high. This is also the only location in the surveyed portion of the Gakkel Ridge where the axis is marked by a volcanic ridge. The axial high and across-axis ridge are associated with a large negative MBA gravity anomaly which implies about 3 km of crustal thickening (Figures 10 and 11). This short length of the axis appears to be characterized by volcanic and tectonic processes typical of the MAR axis and has generated a multiple kilometer thick crustal section. The crust in this portion of the Gakkel Ridge probably consists of a ''typical'' oceanic crustal section including gabbros, dikes, and the basaltic flows and small volcanoes visible at the surface.

4. Barring a major threshold effect change in melt production and/or mantle flow with decreasing spreading rate, the most probable reason for the very different nature of magmatic activity east and west of 32°E is a difference in the mantle source. A likely explanation is interaction of the ridge axis with a passively imbedded chemical heterogeneity in the mantle centered under 19°E. Early melting of the heterogeneity may encourage inflow and focusing of melt over the inhomogeneity [*Michael et al.*, 1994]. Focusing of melt from a large region to 19°E is suggested by the almost complete lack of any other volcanism along the ridge for 275 km from 3°E to 32°E. If this hypothesis is correct, enriched basalts should be observed in the 19°E area.

5. The ridge axis is continuous with no transform offsets throughout the mapped region. However, sections of the ridge axis show distinctly different linear trends. Changes in ridge trend at 32°E and 63°E are associated with very similar bathymetric features which share a number of characteristics with each other and with inside/outside corner complexes observed at the MAR. The most prominent morphologic feature is a shallow, highstanding ridge extending away from the axis on the ''inside'' corner. Gravity data shows that the crust is not thickened under these very shallow ridges and that they are tectonic rather

than volcanic in origin. The fact that nearly identical morphology is found at these changes in ridge axis trend indicates that this morphology arises from tectonics related to the change in trend. These ridges are closely analogous to the inside corner ridges observed at MAR ridge discontinuities. At the MAR, these ridges are the footwall of shallow-dipping detachment faults. The changes in ridge axis trend at the Gakkel Ridge may also be accompanied by detachment faulting.

[66] **Acknowledgments.** We thank Captain R. Perry, the officers and crew of the USS *Hawkbill*, and the scientists and engineers who sailed on the SCICEX98 and SCICEX99 cruises. Dale Chayes and Mark Rognstad played important roles in the development of the SCAMP instrument package and Roger Davis led the development of processing software. SCAMP was funded by the National Science Foundation, the Lamont-Doherty Earth Observatory of Columbia University, the Palisades Geophysical Institution and the governments of Canada, Norway, and Sweden. This research was funded by National Science Foundation grants OPP-96-18436, OPP-98-13540 (JRC), OPP-96-19251, OPP-98-13560 (MHE), and OPP-99-06149 (BJC). LDEO contribution 6407, SOEST contribution 6089.

References

Bell, R. E., and A. B. Watts, Evaluation of the BGM-3 sea gravity meter system onboard R/V *Conrad*, *Geophysics*, *51*, 1480–1493, 1986.

Bergh, H. W., and I. O. Norton, Prince Edward fracture zone and the evolution of the Mozambique Ridge, *J. Geophys. Res.*, *81*, 5221–5239, 1976.

Blackman, D. K., and D. W. Forsyth, Isostatic compensation of tectonic features of the Mid-Atlantic Ridge: 25–27°S, *J. Geophys. Res.*, *96*, 11,741–11,758, 1991.

Blackman, D. K., J. R. Cann, B. Janssen, and D. K. Smith, Origin of extensional core complexes: Evidence from the Mid-Atlantic Ridge at Atlantis Fracture Zone, *J. Geophys. Res.*, *103*, 21,315–21,333, 1998.

Bown, J. W., and R. S. White, Variation with spreading rate of oceanic crustal thickness and geochemistry, *Earth Planet. Sci. Lett.*, *121*, 435–449, 1994.

Brown, J. R., and J. A. Karson, Variations in axial processes on the Mid-Atlantic Ridge: The median valley of the MARK area, *Mar. Geophys. Res.*, *10*, 109–138, 1988.

Carbotte, S. M., and K. C. Macdonald, The axial topographic high at intermediate and fast spreading ridges, *Earth Planet. Sci. Lett.*, *128*, 85–97, 1994a.

Carbotte, S. M., and K. C. Macdonald, Comparison of seafloor tectonic fabric at intermediate, fast, and super fast spreading ridges: Influence of spreading rate, plate motions, and ridge segmentation on fault patterns, *J. Geophys. Res.*, *99*, 13,609–13,631, 1994b.

Chayes, D. N., B. J. Coakley, M. G. Langseth, R. M. Anderson, G. DiBella, M. R. Rognstad, R. B. Davis, M. H. Edwards, J. G. Kosalos, and S. J. Szender, SCAMP: An enhanced geophysical mapping system for Arctic submarine cruises, *Eos Trans. AGU*, *77*, F315, 1996.

Chayes, D. N., R. M. Anderson, J. L. Ardai, B. J. Coakley, R. B. Davis, M. H. Edwards, and M. R. Rognstad, SCAMP performance, *Eos Trans. AGU*, *80*, F1001, 1999.

Chen, Y. J., Oceanic crustal thickness versus spreading rate, *Geophys. Res. Lett.*, *8*, 753–756, 1992.

Chen, Y. J., and W. J. Morgan, Rift valley/no rift valley transition at mid-ocean ridges, *J. Geophys. Res.*, *95*, 17,571–17,581, 1990.

Coakley, B. J., and J. R. Cochran, Gravity evidence of very thin crust at the Gakkel Ridge (Arctic Ocean), *Earth Planet. Sci. Lett.*, *162*, 81–95, 1998.

Cochran, J. R., and B. J. Coakley, Morphology and segmentation of the Gakkel Ridge, Arctic Ocean, from SCICEX data (Abst.), *Eos Trans. AGU*, *79*, F854, 1998.

DeMets, C., R. G. Gordon, D. F. Argus, and S. Stein, Effect of recent revisions to the geomagnetic reversal time scale on estimates of current plate motions, *Geophys. Res. Lett.*, *21*, 2191–2194, 1994.

Detrick, R. S., H. D. Needham, and V. Renard, Gravity anomalies and crustal thickness variations along the Mid-Atlantic Ridge between 33°N and 40°N, *J. Geophys. Res.*, *100*, 3767–3787, 1995.

Dick, H. J. B., G. J. Kurras, J. Snow, W. Jokat, P. Michael, and C. Langmuir, Volcanic and tectonic processes along the Gakkel Ridge: Morphologic interpretation of axial valley features and samples from the Arctic Mid-Ocean Ridge Expedition (AMORE) (Abst.), *Eos Trans. AGU*, *82*, F1098, 2001.

Duckworth, G. L., A. B. Baggeroer, and H. R. Jackson, Crustal structure measurements near FRAM II in the Pole Abyssal Plain, *Tectonophysics*, *89*, 172–215, 1982.

Edwards, M. H., G. J. Kurras, M. Tolstoy, D. R. Bohnenstiehl, B. J. Coakley, and J. R. Cochran, Evidence of recent volcanic activity on the ultra-slow-spreading Gakkel Ridge, *Nature*, *409*, 808–812, 2001.

Feden, R. H., P. R. Vogt, and H. S. Fleming, Magnetic and bathymetric evidence for the "Yermak hot spot" northwest of Svalbard in the Arctic Basin, *Earth Planet. Sci. Lett.*, *44*, 18–38, 1979.

Fisher, R. L., and J. G. Sclater, Tectonic evolution of the Southwest Indian Ocean since the Mid-Cretaceous: Plate motions and stability of the pole of Antarctica/Africa for at least 80 m.g.r., *Geophys. J. R. Astron. Soc.*, *73*, 553–576, 1983.

Fox, P. J., N. R. Grindlay, and K. C. Macdonald, The Mid-Atlantic Ridge (31°S–34°30′S): Temporal and spatial variations of accretionary processes, *Mar. Geophys. Res.*, *13*, 1–20, 1991.

Hooft, E. E. E., R. S. Detrick, D. R. Toomey, J. A. Collins, and J. Lin, Crustal thickness and structure along three contrasting spreading segments of the Mid-Atlantic Ridge, 33.5°E–35°E, *J. Geophys. Res.*, *105*, 8205–8226, 2000.

Jackson, H. R., I. Reid, and R. K. H. Falconer, Crustal structure near the Arctic Mid-Ocean Ridge, *J. Geophys. Res.*, *87*, 1773–1783, 1982.

Jackson, H. R., D. A. Forsyth, J. K. Hall, and A. Overton, Seismic reflection and refraction, in *The Arctic Ocean Region*, edited by A. Grantz et al., pp. 153–170, Geol. Soc. of Am., Boulder, Colo., 1990.

Jakobsson, M., N. Cherkis, J. Woodward, R. McNab, and B. Coakley, New grid of Arctic bathymetry aids scientists and mapmakers, *Eos Trans. AGU*, *81*, 89–96, 2000.

Johnson, G. L., Morphology of the Eurasian Arctic Basin, *Polar Rec.*, *14*, 619–628, 1969.

Johnson, G. L., and B. C. Heezen, The Arctic Mid-Ocean Ridge, *Nature*, *215*, 724–725, 1967.

Johnson, G. L., A. Grantz, and J. R. Weber, Bathymetry and physiography, in *The Arctic Ocean Region*, edited by A. Grantz et al., pp. 63–78, Geol. Soc. of Am., Boulder, Colo., 1990.

Jokat, W., E. Weigelt, Y. Kristoffersen, T. Rasmussen, and T. Schöne, New geophysical results from the south-western Eurasian Basin (Morris Jessup Rise, Gakkel Ridge, Yermak Plateau) and the Fram Strait, *Geophys. J. Int.*, *123*, 601–610, 1995.

Kovacs, L. C., C. Bernero, G. L. Johnson, R. H. Pilger, S. P. Srivastava, P. T. Taylor, G. E. Vink, and P. R. Vogt, *Residual Magnetic Anomaly Chart of the Arctic Ocean Region*, Geol. Soc. of Am., Boulder, Colo., 1985.

Kristoffersen, Y., Eurasia basin, in *The Arctic Ocean Region*, edited by A. Grantz et al., pp. 365–378, Geol. Soc. of Am., Boulder, Colo., 1990.

Kuo, B. Y., and D. W. Forsyth, Gravity anomalies of the ridge-transform system in the south Atlantic between 31 and 34.5°S: Upwelling centers and variations in crustal thickness, *Mar. Geophys. Res.*, *10*, 205–232, 1988.

Kurras, G. J., M. H. Edwards, J. R. Cochran, and B. J. Coakley, Tectonism and volcanism along the Gakkel mid-ocean ridge (5°–74°E): Initial processing and analysis of SCAMP Sidescan data from SCICEX '98 and '99, *Eos Trans. AGU*, *80*, F998, 1999.

Kurras, G. J., M. H. Edwards, R. M. Anderson, P. Michael, J. R. Cochran, and B. J. Coakley, Comparison of Seabeam 2112 and SCAMP bathymetry data along the Gakkel Ridge: Preliminary mapping results from the Healy0102 cruise, in *Oceans 2001 MTS/IEEE Proceedings*, pp. 1496–1499, Inst. of Electr. and Electron. Eng., Washington, D.C., 2001.

Langmuir, C. H., K. Lehnert, S. L. Goldstein, P. Michael, D. Graham, and B. Schramm, Petrology of Gakkel Ridge basalts: Preliminary results, *Eos Trans. AGU*, *82*, F1098–F1099, 2001.

Lin, J., G. M. Purdy, H. Schouten, J. C. Sempere, and C. Zervas, Evidence from gravity data for focused magmatic accretion along the Mid-Atlantic Ridge, *Nature*, *344*, 627–632, 1990.

Macdonald, K. C., P. J. Fox, R. T. Alexander, R. Pockalny, and P. Gente, Volcanic growth faults and the origin of Pacific abyssal hills, *Nature*, *380*, 125–129, 1996.

Michael, P. J., et al., Mantle control of a dynamically evolving spreading center: Mid-Atlantic Ridge 31–34°S, *Earth Planet. Sci. Lett.*, *121*, 451–468, 1994.

Minshull, T. A., Along-axis variations on oceanic crustal density an their contribution to gravity anomalies at slow-spreading ridges, *Geophys. Res. Lett.*, *23*, 849–852, 1996.

Müller, C., and W. Jokat, Seismic evidence for volcanic activity discovered in the central Arctic, *Eos Trans. AGU*, *81*, 265–269, 2000.

Mutter, J. C., and J. A. Karson, Structural processes at slow-spreading ridges, *Science*, *257*, 627–634, 1992.

Ostenso, N. A., and R. J. Wold, Aeromagnetic evidence for origin of Arctic Ocean Basin, in *Arctic Geology*, edited by M. G. Pitcher, pp. 506–516, Am. Assoc. of Pet. Geol., Tulsa, Okla., 1973.

Pariso, J. E., J. C. Sempere, and C. Rommevaux, Temporal and spatial variations in crustal accretion along the Mid-Atlantic Ridge (29°N–31°N) over the last 10 m.y.: Implications from a three-dimensional gravity study, *J. Geophys. Res.*, *100*, 17,781–17,794, 1995.

Parker, R. L., The rapid calculation of potential anomalies, *Geophys. J. R. Astron. Soc.*, *31*, 447–455, 1973.

Patriat, P., *Reconstitution de l'evolution du systeme de dorsales de l'ocean Indien par les methodes de la Cinematique des Plaques*, 310 pp., Territ. des Terres Australes et Antarctiques Fr., Paris, 1987.

Phipps Morgan, J., and Y. J. Chen, Dependence of ridge-axis morphology on magma supply and spreading rate, *Nature*, *364*, 706–708, 1993.

Phipps Morgan, J., and D. W. Forsyth, Three-dimensional flow and temperature perturbations due to a transform offset: Effects on oceanic crustal and upper mantle structure, *J. Geophys. Res.*, *93*, 2955–2966, 1988.

Prince, R. A., and D. W. Forsyth, Horizontal extent of anomalously thin crust near the Vema Fracture Zone from the three-dimensional analysis of gravity anomalies, *J. Geophys. Res.*, *93*, 8051–8063, 1988.

Reid, I., and H. R. Jackson, Oceanic spreading rate and crustal thickness, *Mar. Geophys. Res.*, *5*, 165–172, 1981.

Rommevaux-Jestin, C., N. R. Grindlay, J. A. Madsen, and J. Sclater, Magnetic and kinematic study at the Southwest Indian Ridge between 15°E and 35°E (Abst.), *Eos Trans. AGU*, *77*, F689, 1996.

Sempere, J. C., G. M. Purdy, and H. Schouten, Segmentation of the Mid-Atlantic Ridge between 24°N and 30°40′N, *Nature*, *344*, 427–431, 1990.

Sempere, J. C., J. Lin, H. S. Brown, H. Schouten, and G. M. Purdy, Segmentation and morphologic variations along a slow-spreading center: The Mid-Atlantic Ridge (24°00′N–30°40′N), *Mar. Geophys. Res.*, *15*, 153–200, 1993.

Severinghaus, J. P., and K. C. Macdonald, High inside corners at ridge-transform intersections, *Mar. Geophys. Res.*, *9*, 353–367, 1988.

Smith, D. K., and J. R. Cann, Hundreds of small volcanoes on the median valley floor of the Mid-Atlantic Ridge at 24–30°N, *Nature*, *348*, 152–155, 1990.

Smith, D. K., and J. R. Cann, The role of seamount volcanism in crustal construction at the Mid-Atlantic Ridge (24°–30°N), *J. Geophys. Res.*, *97*, 1645–1658, 1992.

Smith, D. K., and J. R. Cann, Building the crust at the Mid-Atlantic Ridge, *Nature*, *365*, 707–715, 1993.

Smith, D. K., J. R. Cann, M. E. Dougherty, J. Lin, S. Spencer, C. MacLeod, K. J. E. McAllisrwe, B. Brooks, R. Pascoe, and W. Robertson, Mid-Atlantic Ridge volcanism from deep-towed side-scan sonar images, 25°–29°N, *J. Volcanol. Geotherm. Res.*, *67*, 232–262, 1995.

Sparks, D. W., and E. M. Parmentier, The generation and migration of partial melt beneath oceanic spreading centers, in *Magmatic Systems*, edited by M. P. Ryan, pp. 55–76, Academic, San Diego, Calif., 1994.

Tolstoy, M., A. J. Harding, and J. A. Orcutt, Crustal thickness on the Mid-Atlantic Ridge: Bull's eye gravity anomalies and focused accretion, *Science*, *262*, 726–729, 1993.

Tolstoy, M., D. R. Bohnenstiehl, M. H. Edwards, and G. J. Kurras, Seismic character of volcanic activity at the ultraslow-spreading Gakkel Ridge, *Geology*, *29*, 1139–1142, 2001.

Tucholke, B. E., and J. Lin, A geologic model for the structure of ridge segments in slow-spreading ocean crust, *J. Geophys. Res.*, *99*, 11,937–11,958, 1994.

Vogt, P. R., P. T. Taylor, L. C. Kovacs, and G. L. Johnson, Detailed aeromagnetic investigation of the Arctic Basin, *J. Geophys. Res.*, *84*, 1071–1089, 1979.

Weissel, J. K., and G. Karner, Flexural uplift of rifts flanks due to mechanical unloading of the lithosphere during extension, *J. Geophys. Res.*, *94*, 13,919–13,950, 1989.

White, R. S., D. McKenzie, and R. K. O'Nions, Oceanic crustal thickness from seismic measurements and rare earth element inversions, *J. Geophys. Res.*, *97*, 19,683–19,715, 1992.

B. J. Coakley, Geophysical Institute, University of Alaska Fairbanks, Fairbanks, AK, USA.

J. R. Cochran, Lamont-Doherty Earth Observatory of Columbia University, Palisades, NY, USA. (jrc@ldeo.columbia.edu)

M. H. Edwards, Hawaii Institute of Geophysics and Planetology, School of Ocean and Earth Science and Technology, University of Hawaii, Honolulu, HI, USA.

G. J. Kurras, Department of Geology and Geophysics, School of Ocean Earth Science and Technology, University of Hawaii, Honolulu, HI, USA.

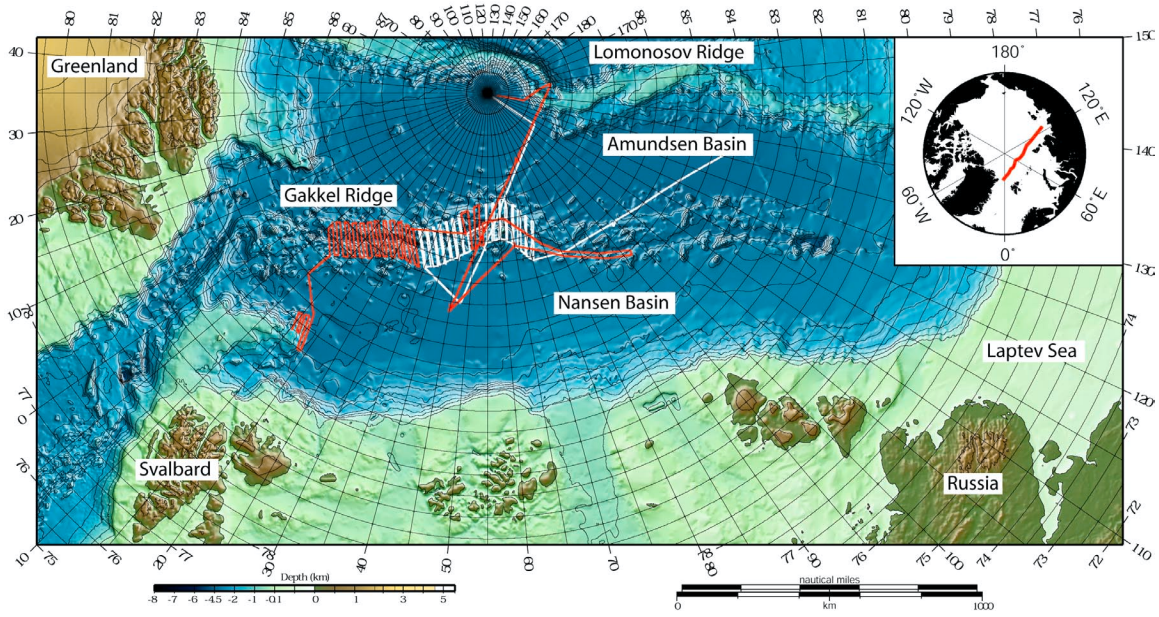

Figure 1. Bathymetric map of the Eurasian Basin showing the location of the Gakkel Ridge and tracks of the USS Hawkbill cruises, which collected the data on which this report is based. The 1998 cruise is shown in white and the 1999 cruise in red. Bathymetry is from the International Bathymetric Chart of the Arctic (IBCAO) database [Jakobsson et al., 2000]. The inset shows the location of the Gakkel Ridge within the entire Arctic Ocean.

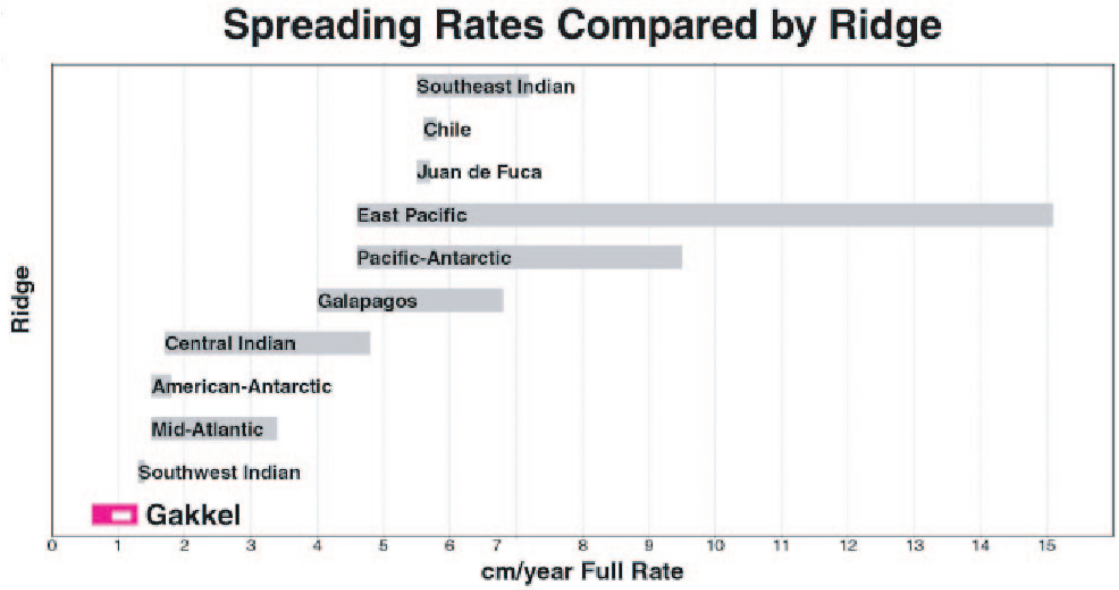

Figure 2. Spreading rates of different portions of the global mid-ocean system [DeMets et al., 1994]. The white line within the Gakkel Ridge bar shows the range of spreading rates within our study area.

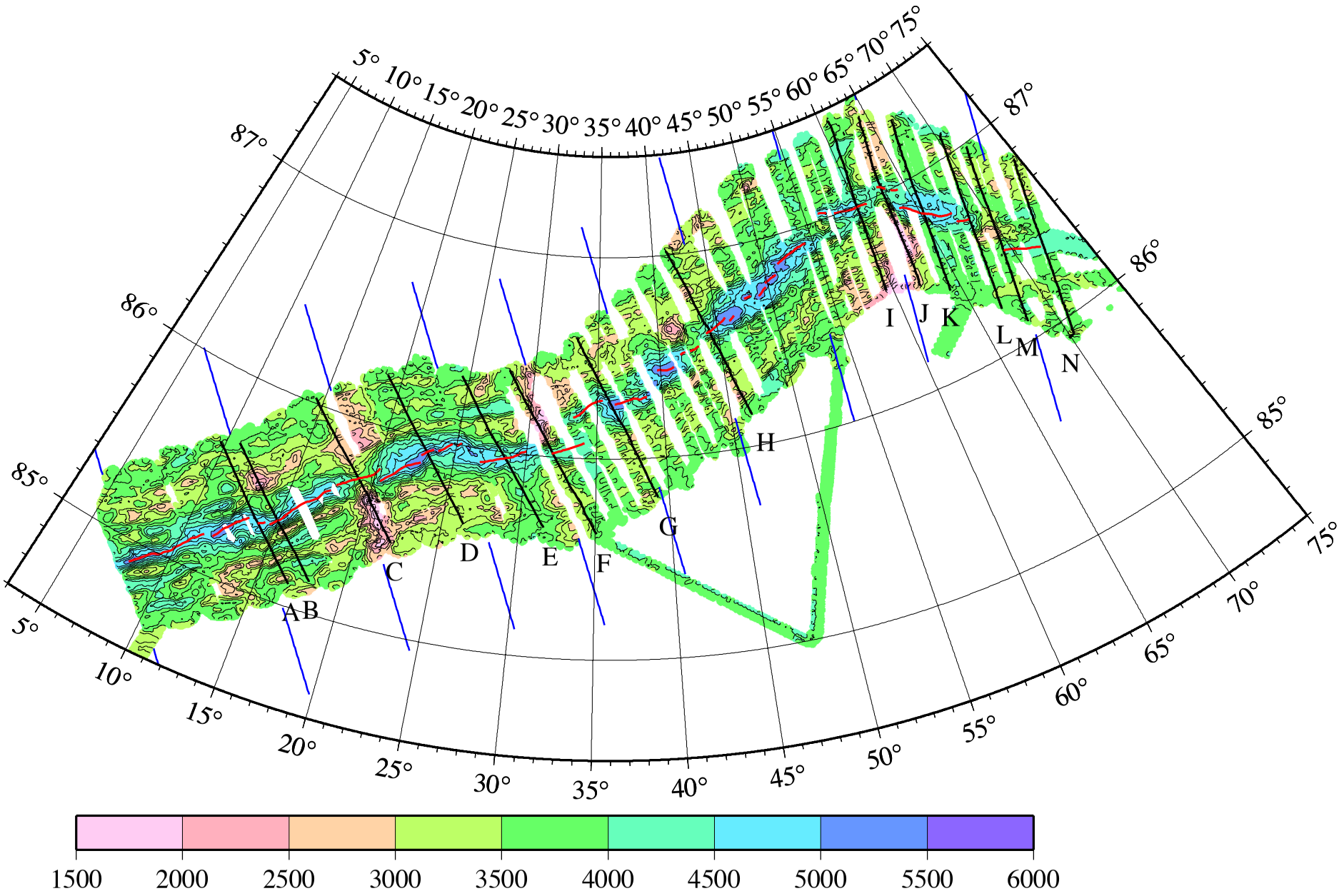

Figure 3. Bathymetry map of the western Gakkel Ridge based on gridded SCAMP bathymetry data obtained by USS Hawkbill during the 1998 and 1999 SCICEX cruises. Contour interval is 250 m with color changes at 500 m intervals. The location of the ridge axis is shown by a bold line. Solid lines outside the mapped area are parallel to the spreading direction. Solid lines on the map show ship tracks for profiles shown in Figure 6. Letters next to tracks correspond to those in Figure 6.

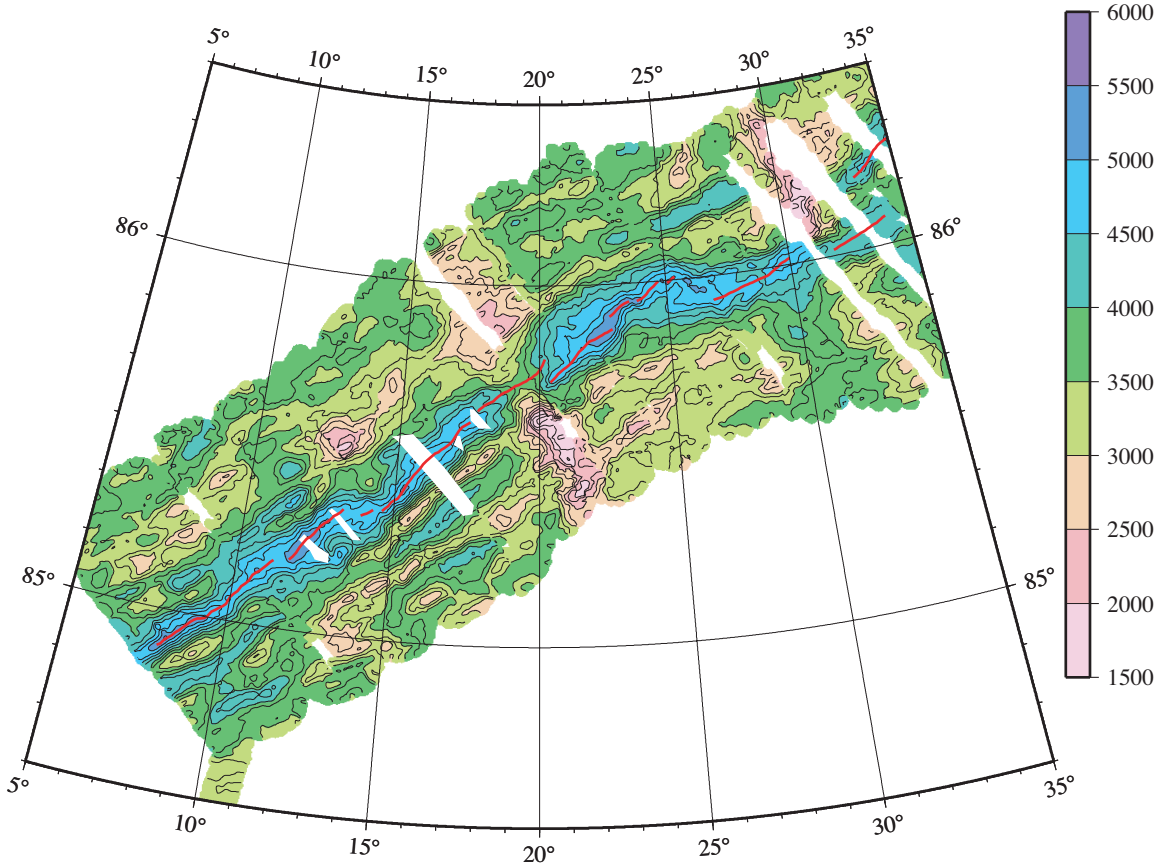

Figure 4a. Bathymetry map of the Gakkel Ridge from 5_E to 35_E based on gridded SCAMP bathymetry data obtained by USS Hawkbill during the 1998 and 1999 SCICEX cruises. Contour interval is 250 m with color changes at 500 m intervals. The bold line shows the location of the ridge axis.

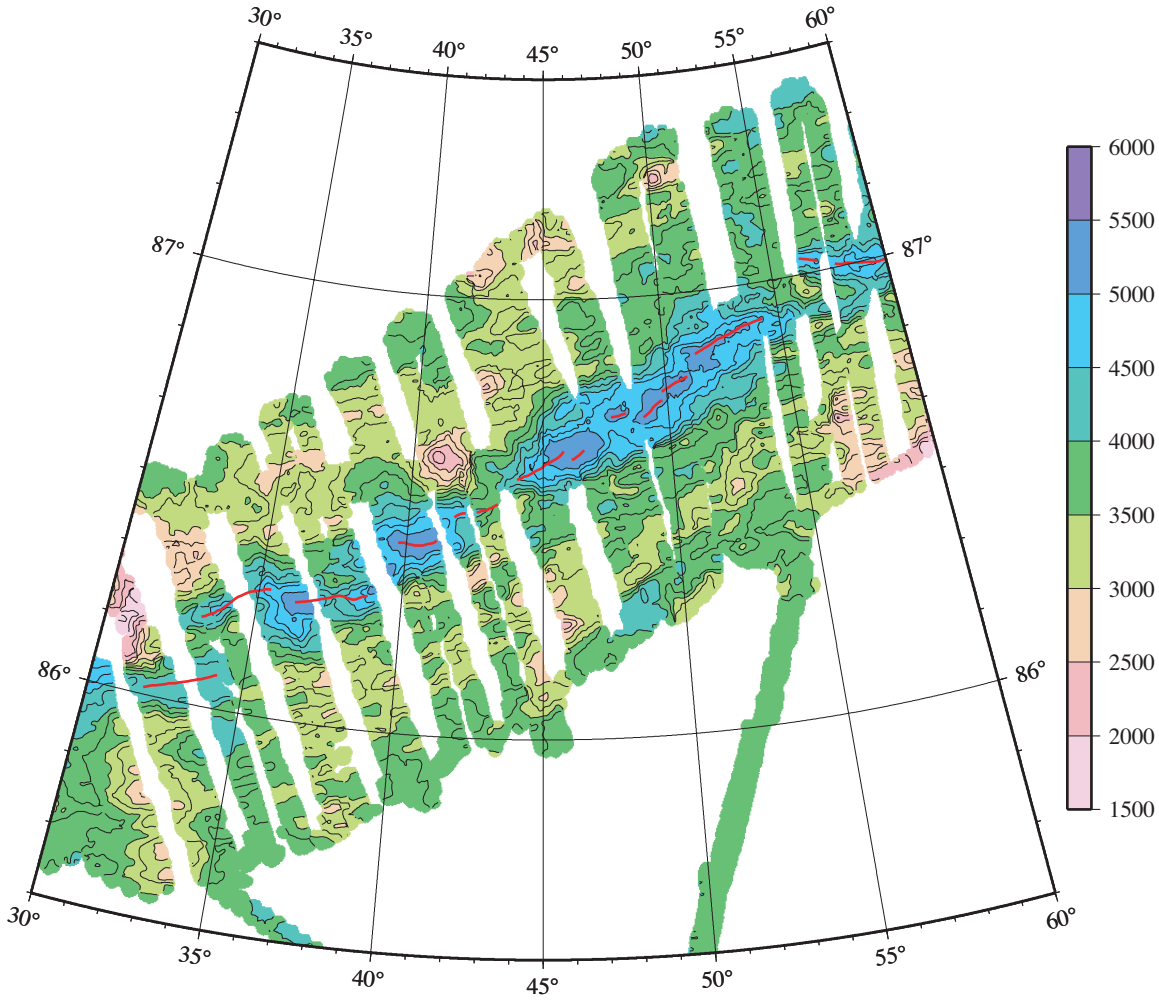

Figure 4b. Bathymetry map of the Gakkel Ridge from 30_E to 60_E based on gridded SCAMP bathymetry data obtained by USS Hawkbill during the 1998 and 1999 SCICEX cruises. Contour interval is 250 m with color changes at 500 m intervals. The bold line shows the location of the ridge axis.

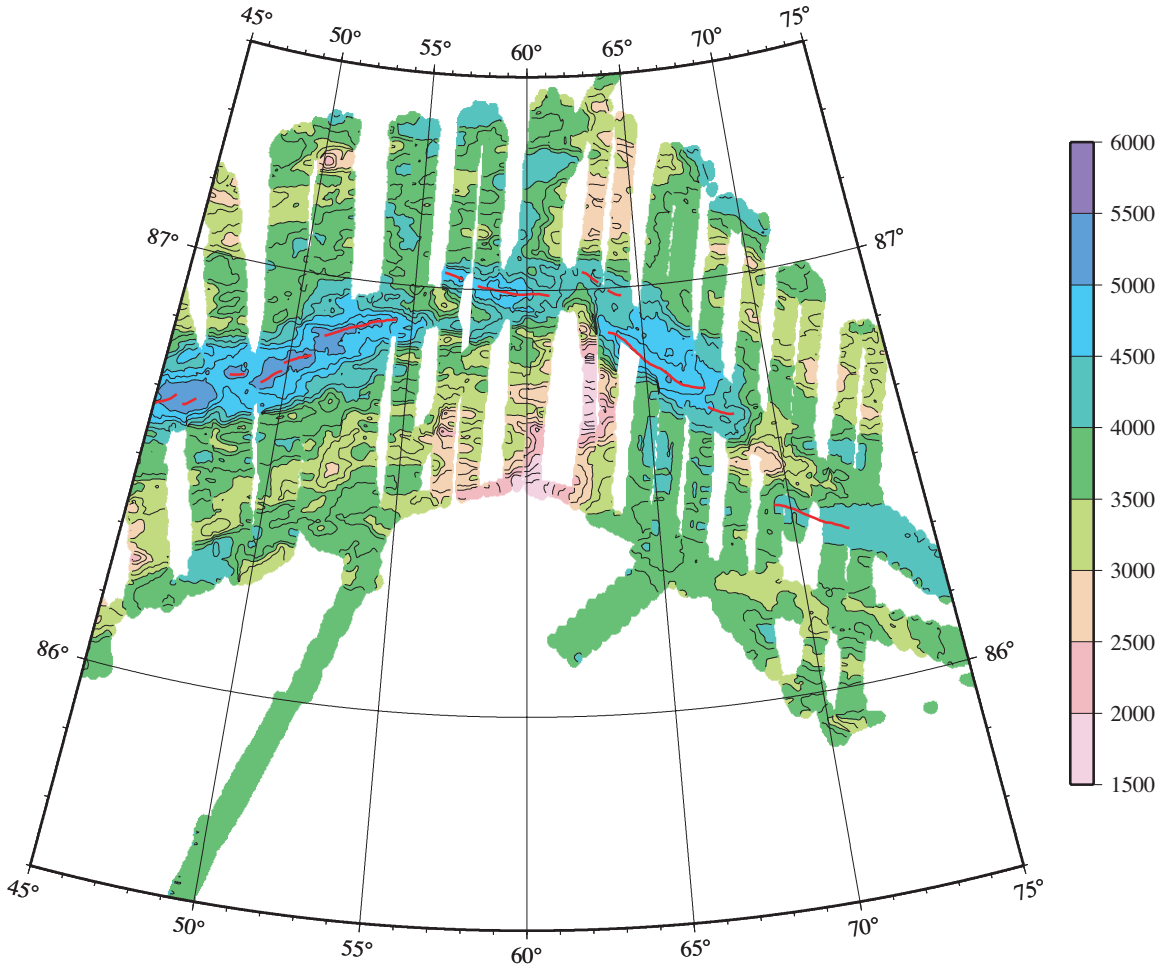

Figure 4c. Bathymetry map of the Gakkel Ridge from 55_E to 75_E based on gridded SCAMP bathymetry data obtained by USS Hawkbill during the 1998 and 1999 SCICEX cruises. Contour interval is 250 m with color changes at 500 m intervals. The bold line shows the location of the ridge axis.

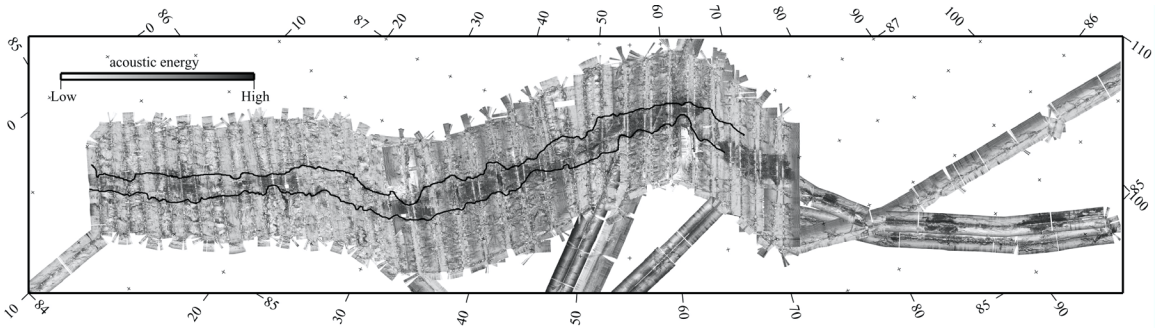

Figure 5. Side scan map of the Gakkel Ridge from 5_E to 98_E based on SCAMP side scan data obtained by USS Hawkbill during the 1998 and 1999 SCICEX cruises. Black represents very high energy returns and white represents very low energy returns.

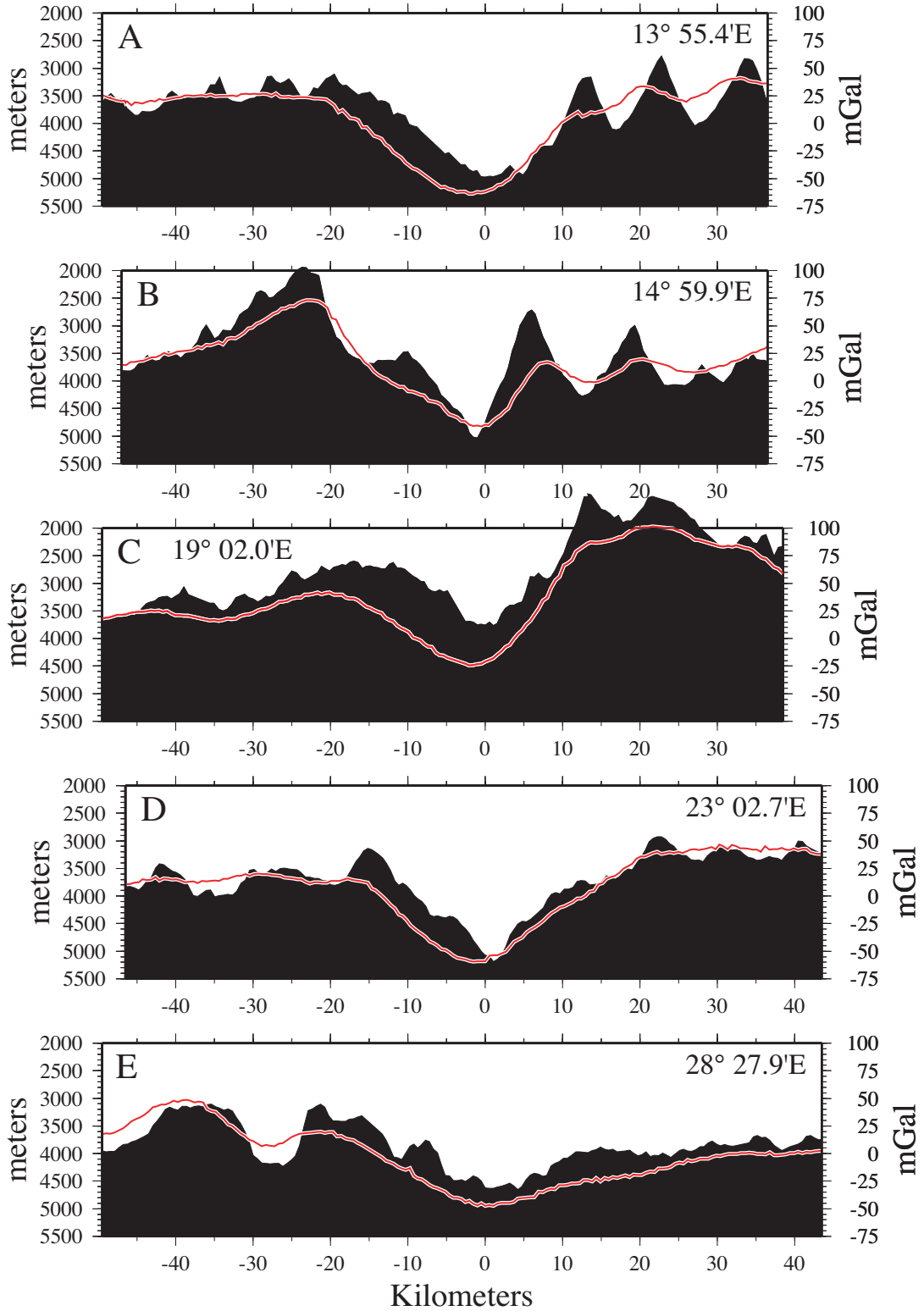

Figure 6. Selected bathymetry and free-water gravity profiles across the Gakkel Ridge. Profiles are projected along the local spreading direction with the axis as the origin. North is to the left (negative distances). The longitude at which each profile crosses the axis is noted. Letters on each profile correspond to those on Figure 3, which shows the locations of the profiles.

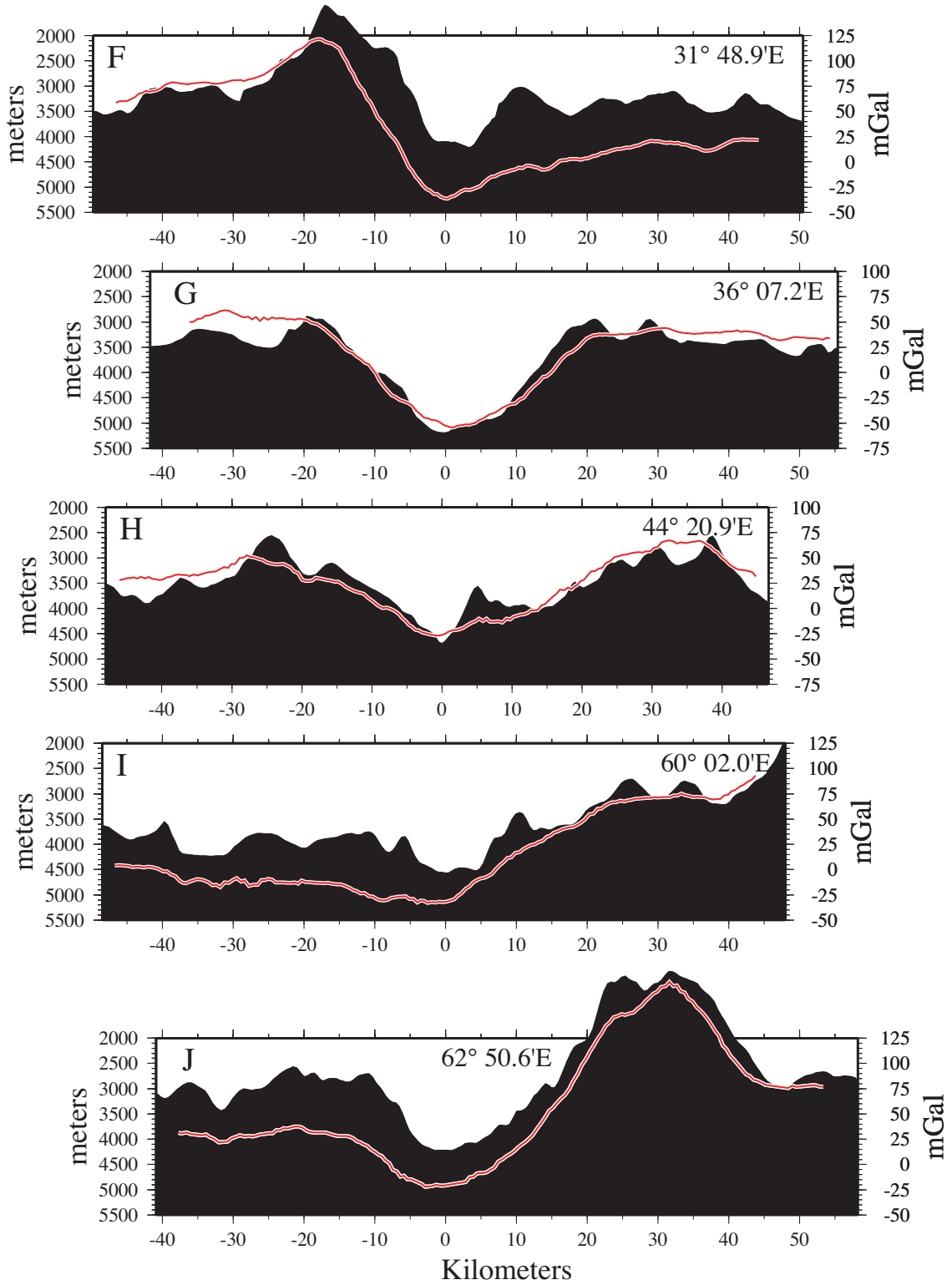

Figure 6 (cont.). Selected bathymetry and free-water gravity profiles across the Gakkel Ridge. Profiles are projected along the local spreading direction with the axis as the origin. North is to the left (negative distances). The longitude at which each profile crosses the axis is noted. Letters on each profile correspond to those on Figure 3, which shows the locations of the profiles.

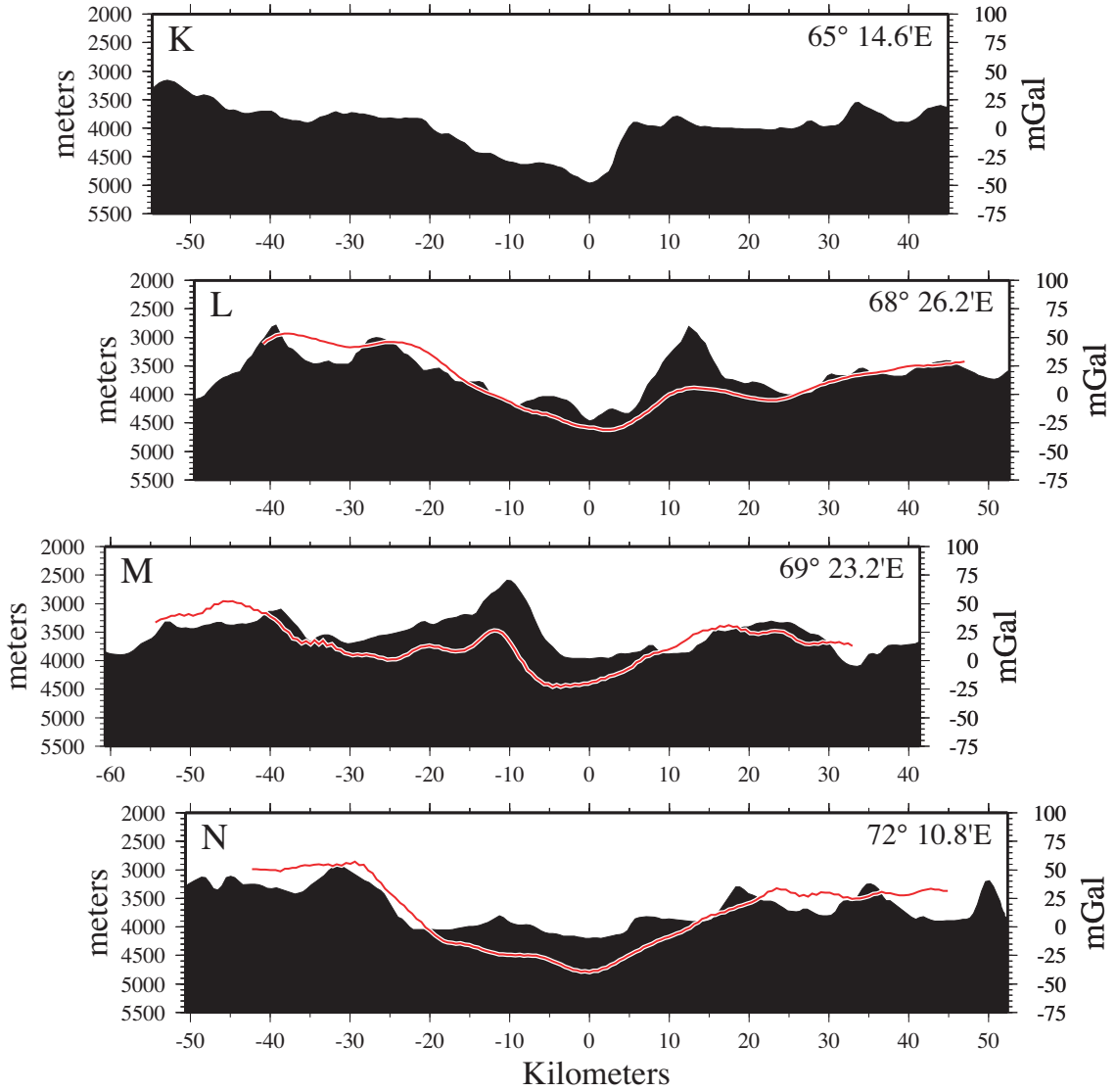

Figure 6 (cont.). Selected bathymetry and free-water gravity profiles across the Gakkel Ridge. Profiles are projected along the local spreading direction with the axis as the origin. North is to the left (negative distances). The longitude at which each profile crosses the axis is noted. Letters on each profile correspond to those on Figure 3, which shows the locations of the profiles.

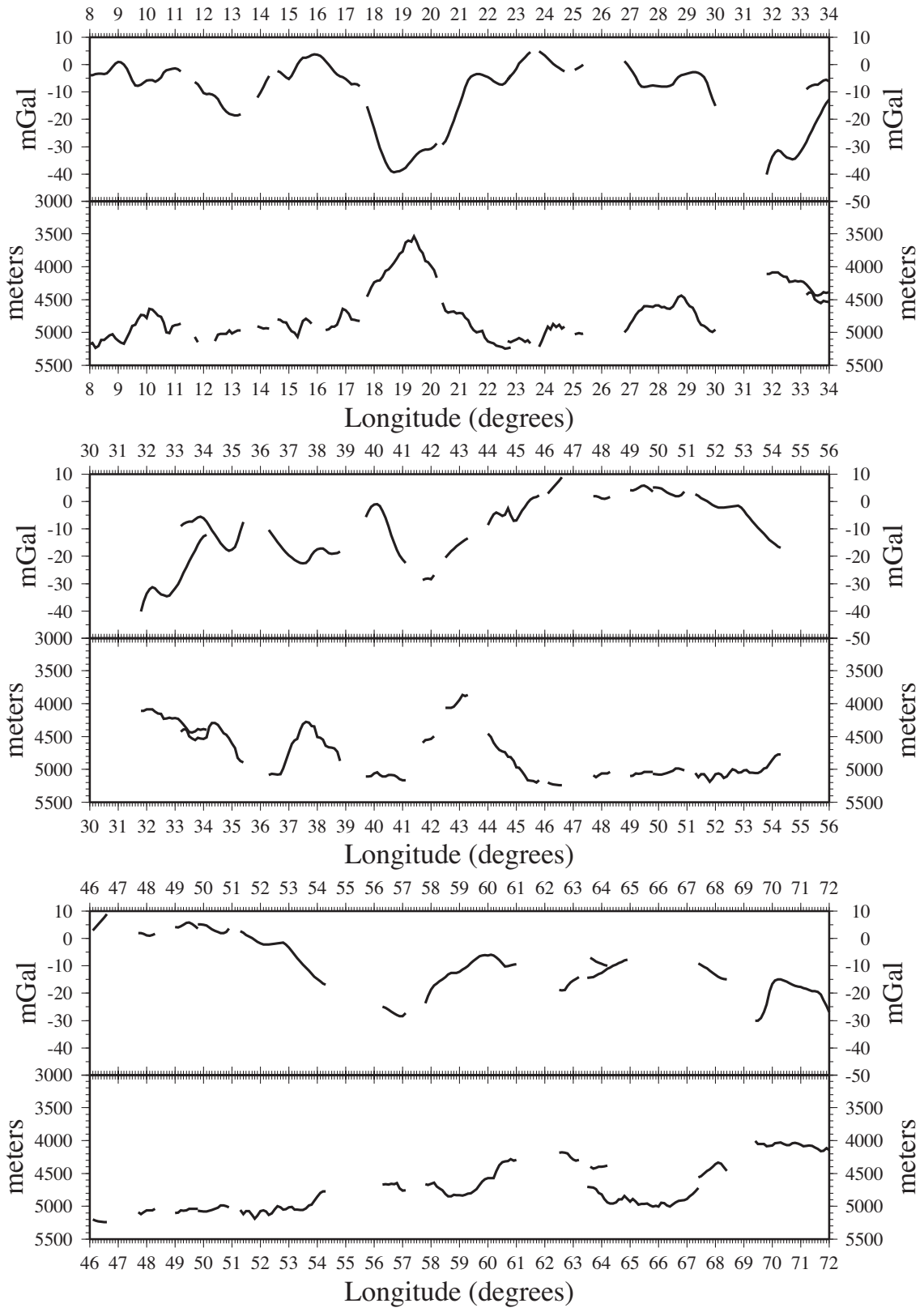

Figure 7. Variations in axial depth and axial mantle Bouguer gravity anomaly along the Gakkel Ridge. Depth is at the bottom and gravity at the top in each panel.

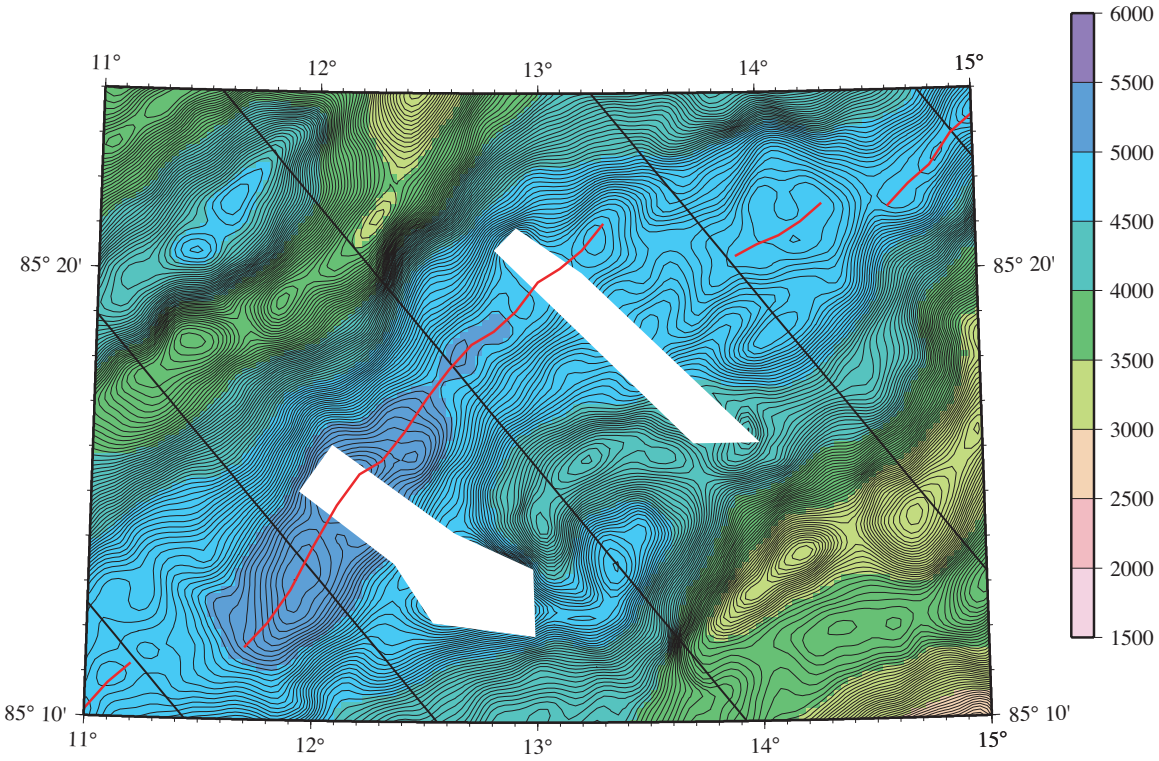

Figure 8. Bathymetry map of the Gakkel Ridge axis from 11_E to 15_E contoured at 25 m intervals. Bold line shows location of the ridge axis. Solid lines running roughly NW-SE are parallel to the spreading direction. Note that the axis is consistently located at the bottom of a valley and that the axis consists of a series of segments nearly orthogonal to the spreading direction connected by oblique accommodation zones.

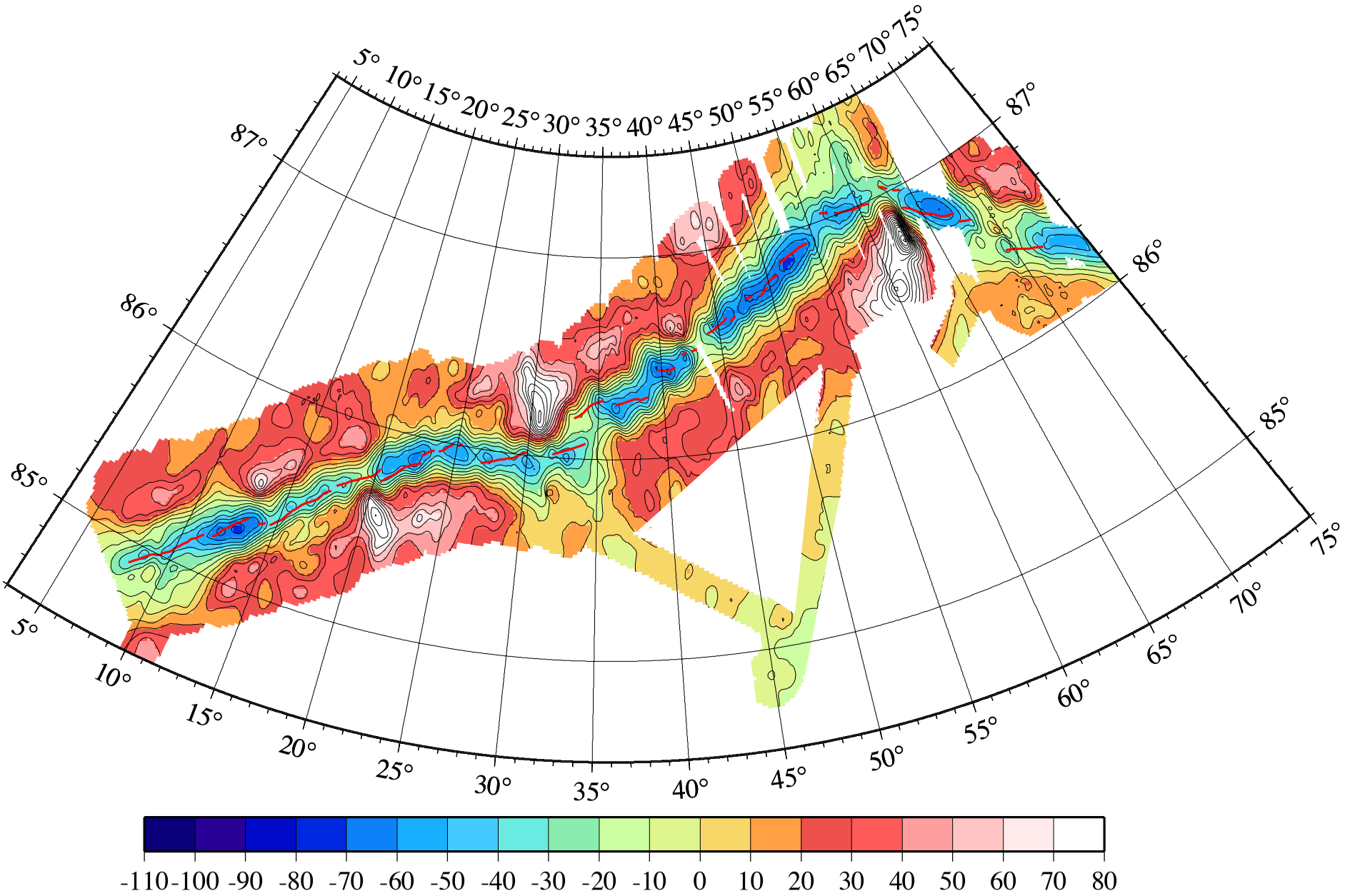

Figure 9. Free-water gravity anomalies over the Gakkel Ridge based on data acquired by USS Hawkbill during the 1998 and 1999 SCICEX cruises. Contour interval is 10 mGal. The bold line shows the location of the ridge axis.

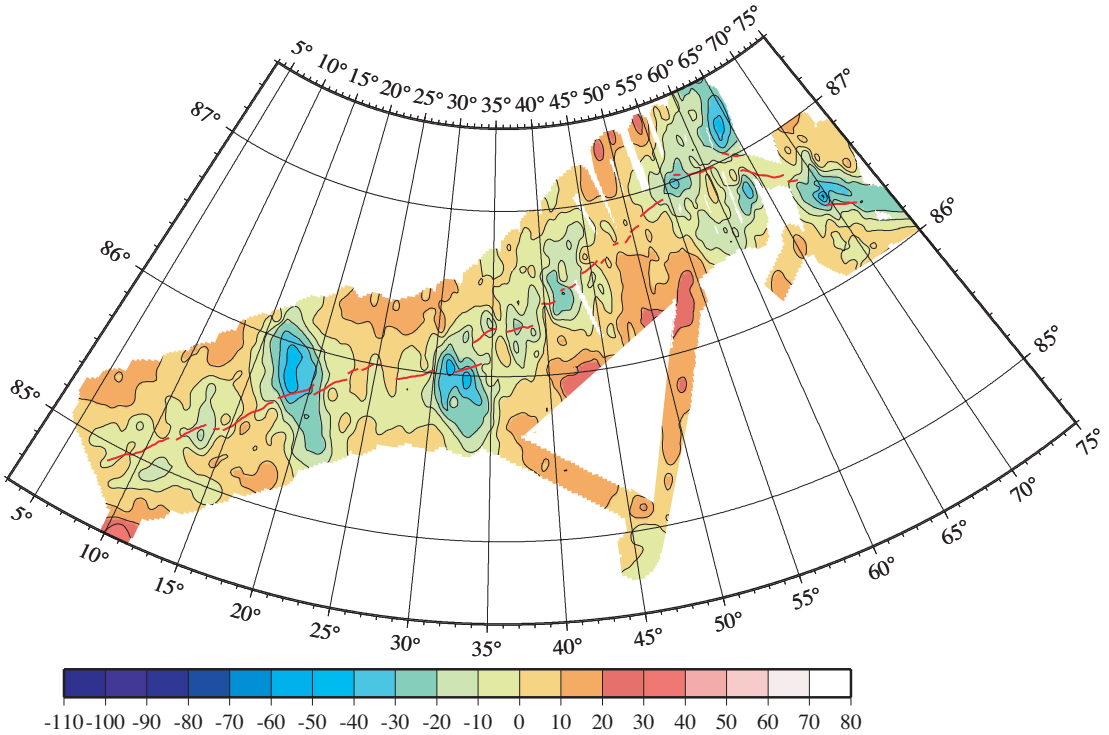

Figure 10. MBAs over the Gakkel Ridge based on data acquired by USS Hawkbill during the 1998 and 1999 SCICEX cruises. The MBA were calculated assuming a 2 km mean crustal thickness [Jackson et al., 1982; Coakley and Cochran, 1998] and density contrasts of 1700 and 600 kg/m3 at the water/crust and crust/mantle interfaces. Contour interval is 10 mGal. The bold line shows the location of the ridge axis.

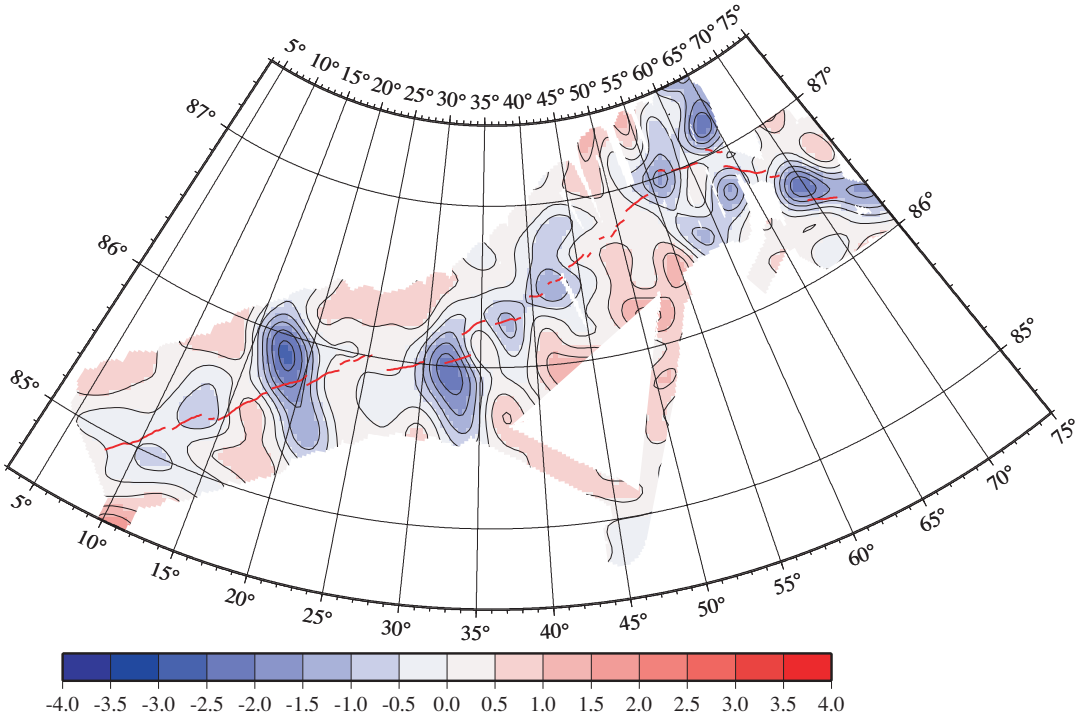

Figure 11. Relative crustal thickness variations calculated by downward continuation of the MBAs (Figure 10). Contour interval is 0.5 km. Negative values denote thicker crust. The bold line shows the location of the ridge axis.

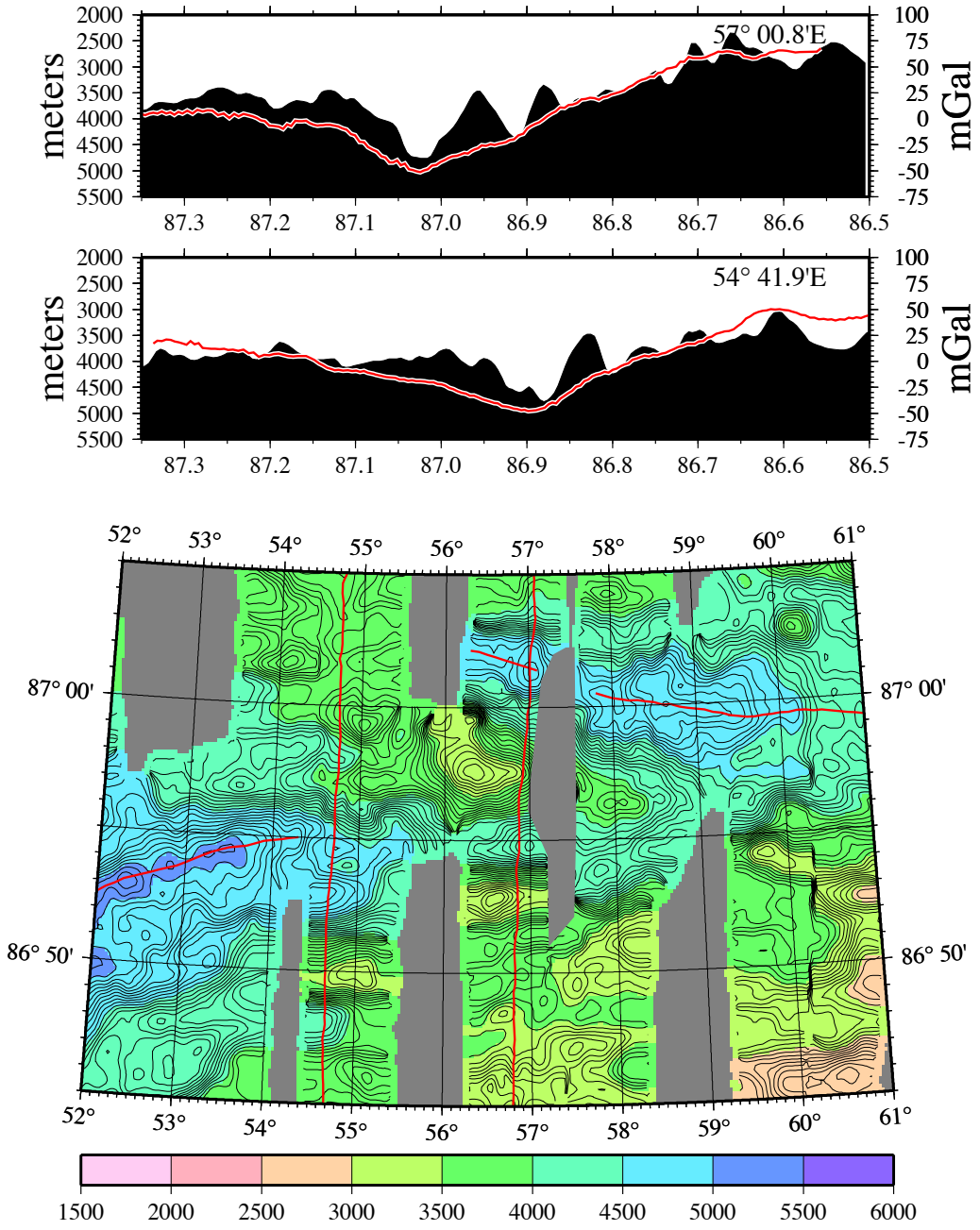

Figure 12. (bottom) Bathymetry map of the Gakkel Ridge axis from 52 E to 61 E based on gridded SCAMP bathymetry data. Contour interval is 50 m with color changes at 500 m intervals. The bold line shows the location of the ridge axis. The location of two bathymetry and free-water gravity anomaly profiles (top) plotted against latitude is also shown on the map. The ridge axis is offset to the north by 14 km between 55 E and 56 E as is clearly demonstrated by the two bathymetric and gravity profiles. There is no bathymetric evidence of a shear zone between the two rift tips. The region of the offset is occupied by a bathymetric high, which appears to be of volcanic origin based on bathymetry and side scan data.

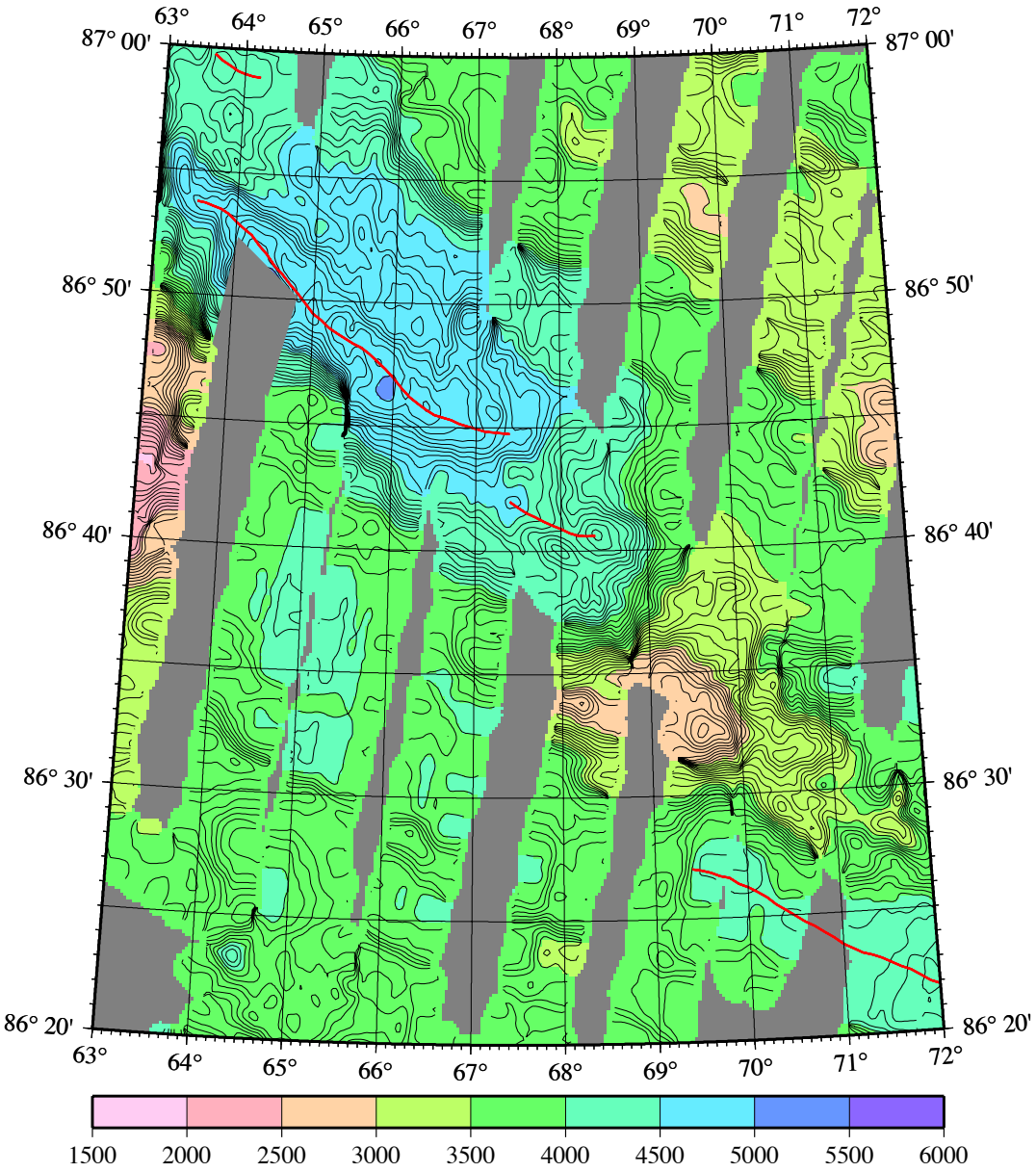

Figure 13. Bathymetry map of the Gakkel Ridge axis from 63 E to 72 E based on gridded SCAMP bathymetry data. Contour interval is 50 m with color changes at 500 m intervals. The bold line shows the location of the ridge axis. The spreading axis steps 18 km to the south near 69 E. The area between the rift tips is occupied by a large bathymetric high, apparently of volcanic origin.